

The author(s) shown below used Federal funds provided by the U.S. Department of Justice and prepared the following final report:

Document Title: Development of a Science Base and Open Source Software for Bloodstain Pattern Analysis

Author(s): Daniel Attinger. Ph.D.

Document No.: 249851

Date Received: April 2016

Award Number: 2010-DN-BX-K403

This report has not been published by the U.S. Department of Justice. To provide better customer service, NCJRS has made this federally funded grant report available electronically.

Opinions or points of view expressed are those of the author(s) and do not necessarily reflect the official position or policies of the U.S. Department of Justice.

Final Technical Report

**Project Title: Development of a Science Base and Open Source Software for Bloodstain
Pattern Analysis**

Award Number: 2010-DN-BX-K403

**Author(s): Dr. Daniel Attinger, Associate Professor
attinger@iastate.edu**

ABSTRACT

The major goals of the project have been to:

- 1) Perform a fundamental and collaborative research to better understand the formation of bloodstains.
- 2) Deliver a knowledge base, innovative measurement methods and pieces of open-source analysis software to help bloodstain pattern analysts better answer the following question: *How was this violent crime committed?*

The main results of the project are a better characterization of the viscosity and surface tension of blood, a novel method to determine the region of origin of a blood spatter, and the fostering of connections between the fluid dynamics community and the bloodstain pattern analysis community.

TABLE OF CONTENTS

Abstract.....	2
Table of Contents.....	3
Executive Summary.....	4
Main Body of the Final Technical Report.....	5
1. Introduction.....	5
2. Methods.....	7
2.1. Reconstruction of curved trajectories of blood drops from stain inspection in blood spatters.....	7
2.1.1. Mathematical Framework for trajectory reconstruction.....	7
2.1.2. Inspection of stains in three dimensions.....	9
2.2. Single drop impact experiments: dripping drops.....	12
2.3. Single drop impact experiments: microdrops.....	13
2.4. Blood spatter experiments.....	15
2.5. Measurement of the physical properties of blood.....	17
2.5.1. Rheology (shear viscosity).....	17
2.5.2. Equilibrium surface tension of blood.....	17
2.5.3. Hematocrit measurement.....	18
2.6. Low-cost measurement of shear viscosity and equilibrium surface tension.....	18
2.7. Wettability measurements.....	20
2.8. A numerical simulation tool to simulate blood drop impacts.....	21
3. Results and Discussion.....	21
3.1. Reconstruction of curved trajectories of blood drops from stain inspection in blood spatter.....	21
3.2. Determination of impact conditions from stain inspection.....	23
3.2.1. Inspection of stains in three dimensions.....	23
3.2.2. Comparison between stationary and portable 3D microscope.....	25
3.3. Measurement of the physical properties of blood.....	26
3.3.1. Rheology of blood (shear viscosity).....	26
3.3.2. Static surface tension of blood.....	27
3.3.3. Hematocrit measurement.....	28
3.3.4. Wettability Measurements.....	28
3.4. Drop impact experiments: dripping drops.....	29
3.5. Drop impact experiments:microdrops.....	31
3.6. Numerical simulation of blood drop impacts.....	35
3.7. Review of the relations between fluid dynamics and bloodstain pattern analysis.....	44
4. Conclusions.....	46
5. References.....	47
6. Dissemination of Research Findings.....	50

EXECUTIVE SUMMARY

Bloodstains are deterministic signs of a violent crime. Bloodstains help determine how the crime happened, pointing e.g. to the region of origin of a blood spatter. However, Bloodstain Pattern Analysis is not straightforward because the physical relation between blood impact and the resulting bloodstains is non-linear. Indeed, the formation of bloodstains involves a complex fluid (the blood), a subtle interplay of fluid mechanics, heat and mass transfer, in the presence of a deforming free surface, and impact surfaces with diverse values of roughness and wettability. The US National Academies recently advocated [1] for stronger scientific foundations given “the complex nature of fluid dynamics”.

The proposed research team has addressed the specific challenge in Bloodstain Pattern Analysis (BPA) to determine where a blood spatter originates from for the purpose of reconstructing the bloodletting event. As stated in 1939 in Balthazard et al. [2], “*Le problème [of reconstructing trajectories] est très difficile à résoudre*”. Indeed, reconstructing trajectories is still very difficult today. The methods of strings and of the tangent [3] typically used in today’s crime scenes are first-order approach to reconstruct trajectories, by assuming that the droplets travel in straight lines. By neglecting drag and gravity forces, these approaches induce systematic and poorly quantified uncertainties [4]. Very recently, BPA research has proposed techniques to reconstruct curved trajectories based on probabilistic or statistical methods, but none of these methods can satisfactorily predict curved trajectories caused by drag and gravity. In this research project, *the hypothesis that 3D inspection of individual stains provides sufficient information to reconstruct curved trajectories accounting for gravity and drag has been tested.*

A method for trajectory reconstruction has been developed, based on the reconstruction of curved trajectories by estimation of impact conditions from three-dimensional measurements of stains. Based on a set of laboratory experiments analog to the situation of a beating, the method is found to be about 4 times more accurate than the method of strings to determine the region of origin of a blood spatter. The device used to inspect stains in 3D has been modified to be portable, possibly to a crime scene. The method however is based on accurately measuring the shape and minute volume of stains, and currently only works on smooth and non-absorbing surfaces.

To estimate the impact conditions from three-dimensional measurements of stains, it is important to know the physical properties of the blood. This project therefore also delivers measurement of the physical properties of porcine blood, a valid substitute of human blood [5]. Measurements are performed both at equilibrium conditions and in dynamic situations close to those in BPA. A set of innovative and simple tools are proposed to characterize e.g. the shear-thinning viscosity, or the relation between drop spreading upon impact and impact conditions.

A numerical simulation tool has also been developed to describe the impact of blood drops, with a specific consideration of the role of wettability.

A review of the relations between fluid dynamics and bloodstain pattern analysis has also been published, with the purpose to bring together the fluid dynamics and the bloodstain pattern analysis communities, as per the recent wish of the National Academies[1].

MAIN BODY OF THE FINAL TECHNICAL REPORT

1. Introduction

This report describes fundamental and collaborative research to better understand the formation of bloodstains.

Bloodstains are deterministic signs of a violent crime. Bloodstains help determine how the crime happened, pointing e.g. to the region of origin of a blood spatter. However, Bloodstain Pattern Analysis (BPA) is not straightforward because the physical relation between blood impact and the resulting bloodstains is non-linear. Indeed, the formation of bloodstains involves a complex fluid (the blood), a subtle interplay of fluid mechanics, heat and mass transfer, in the presence of a deforming free surface, and impact surfaces with varying roughness and wettability. The US National Academies recently advocated [1] for stronger scientific foundations given “the complex nature of fluid dynamics”.

The proposed research team has addressed the specific challenge in Bloodstain Pattern Analysis (BPA) to determine where a blood spatter originates from for the purpose of reconstructing the bloodletting event. As stated in 1939 in Balthazard et al. [2], “*Le problème [of reconstructing trajectories] est très difficile à résoudre*”. Indeed, reconstructing trajectories is still very difficult today. The methods of strings and of the tangent [3] typically used in today’s crime scenes are first-order approach to reconstruct trajectories, by assuming that the droplets travel in straight lines. By neglecting drag and gravity forces, these approaches induce systematic and poorly quantified uncertainties [4]. Very recently, BPA research has proposed techniques to reconstruct curved trajectories based on probabilistic or statistical methods, but none of these methods can satisfactorily predict curved trajectories caused by drag and gravity.

Our hypothesis is that 3D inspection of individual stains provides sufficient information to reconstruct curved trajectories accounting for gravity and drag has been tested.

The research involves experimental, numerical and theoretical components.

To reconstruct drop trajectories from inspection of the stains, a 3D microscope has been acquired to record three-dimensional scans of stained surfaces, with μm resolution in height. These advances in measurement capabilities (together with knowledge of the physical properties of the blood) allow extracting information from individual bloodstains about the impacting drop size and velocity. This information is then used to reconstruct the curved trajectories of the drops rather than the straight lines usually assumed. We have generated blood spatters involving multiple bloodstains and determined from the bloodstains the region of origin of the blood spatter.

Experimentally, the physical properties of blood such as surface tension and rheology (i.e. shear viscosity) have been characterized in unprecedented depth. This is important because the physical properties of blood are rarely measured in BPA studies [6-12].

During the 2013 IABPA conference, a talk by Elizabeth Williams (from the group of Mike Taylor) demonstrated that very few BPA research studies measured physical properties of the blood such as dynamic viscosity. She reviewed a wide range of BPA studies, and only two research teams [5, 13-16] provided sufficient information on the measured viscosity, while the viscosity was not measured in studies by six other research teams [6-12]. Given the wide range of physical properties of the blood [12, 17], the measurement of viscosity and surface tension is important for two reasons. First, without measurement of the physical properties, it is difficult to assess the uncertainty of the results and conclusions drawn from these studies. Also, these physical properties affect the relation between e.g. the stain size and the impact conditions.

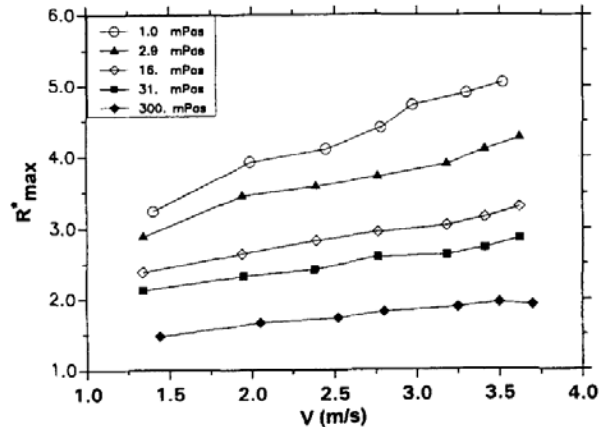


Figure 1: The viscosity of a fluid has a strong influence on the relation between the impact conditions (here the velocity V) ratio of the stain size over the drop size (R^*_{max}). From [18].

A numerical code has been written in the Matlab programming language to determine the region of origin of the blood spatters, using partial or full 3D scans of the spatter. This software reconstructs parabolic trajectories, accounting for drag and gravity forces. Comparisons between the points of origin obtained with the method of strings (state of the art), and 3D inspection of stains have been made.

Numerically, we have also developed a 3D open source numerical code able to describe the fluid dynamics of blood drop impact. This software describes in details the history of the impact of blood drops and the formation of the corresponding stain. This software allows to systematically investigate the influence variables such as the substrate material, drop size, impact velocity and angle.

Theoretically, a review on the relations between bloodstain pattern analysis and fluid dynamics has been written, coauthored with a member of the US National Academy of Engineering. Using dimensional numbers such as the Reynolds and Weber number we have reduced the parameter space and identify general laws governing the impact, splashing and staining process. Some of the knowledge and open-source software developed here has been disseminated via scientific conferences, scientific articles, in active collaboration with a forensic consultant. A specific effort has been put in bringing together the communities of BPA and fluid dynamics/engineering.

2. Methods

2.1. Reconstruction of curved trajectories of blood drops from stain inspection in blood spatters

To find the region of origin of a blood spatter, the state of the art today, called method of the tangent or method of strings, is based on the assumption that drops travel in straight lines. BPA analysts know of this limitation but the estimation of the systematic error and uncertainty is currently only possible for laboratory experiments, not for crime scenes [19-21]. Several improved methods to reconstruct curved trajectories have recently been proposed, based either on ballistic reconstruction [22] or probabilities [23], but they either used unphysical assumptions [24] to determine the impact conditions or neglect [25] important physical aspect of the problem such as the drag. Since ballistic reconstruction involves the knowledge of impact velocity and drop size, a significant amount of recent BPA work has focused on obtaining that information by inspecting the stains.

2.1.1. Mathematical Framework for trajectory reconstruction

The curved trajectories of blood drops can be described mathematically provided the following assumptions are verified:

- a) No interaction between neighboring drops
- b) Negligible buoyancy forces
- c) Negligible lift forces (that is drops are spherical)
- d) Air is at rest
- e) Evaporation during the flight is negligible

When the ratio of the drag force to the gravity force F_d/F_g is not negligible, we obtain the following system of equations for the trajectory of the drop

$$m_d \frac{d\vec{v}}{dt} = m_d \vec{g} - \vec{F}_D, \quad \frac{d\vec{r}}{dt} = \vec{v} \quad (1)$$

where $m_d, \frac{d\vec{v}}{dt}, \vec{g}, \vec{r}$ and \vec{F}_D are the droplet mass, droplet acceleration, gravitational acceleration, droplet position and drag force, respectively.

The value of the drag force is expressed with the correlation

$$\vec{F}_D = \rho_a C_D \frac{A_d}{2} \vec{v}v, \quad (2)$$

where ρ_a, A_d, v and \vec{v} are the air density, the cross-sectional area of the droplet, the velocity magnitude and velocity vector of the droplet. The dimensionless parameter C_D is the drag

coefficient. For BPA cases, C_D is best expressed by the correlation of Lavernia et al. [26], because it is valid for the wide range of aerodynamic situations found in BPA, i.e. for $0.1 \leq Re \leq 4000$:

$$C_D = 0.28 + \frac{6}{Re^{0.5}} + \frac{21}{Re}, \quad (3)$$

In Eq. (1) the last term on the right-hand side accounts for the air drag. Solutions of this equation are subject to the initial conditions

$$t = 0: \quad \mathbf{r} = \mathbf{r}_0, \quad \frac{d\mathbf{r}}{dt} = \mathbf{V}_0, \quad (4)$$

where \mathbf{r}_0 and \mathbf{V}_0 are the radius vector of the point of impact of the drop, and \mathbf{V}_0 is the velocity vector of the impacting drop, respectively.

This system of equations can be integrated backward in time, starting from the impact conditions to reconstruct the curved trajectories of the blood drops [27-29]. The idea is to integrate the ballistic equations backward in time, as in [22] and the figure below. Since the time goes backward, the effect of the drag force term in equation (1) is to effectively increase the energy to the drop along its backward trajectory.

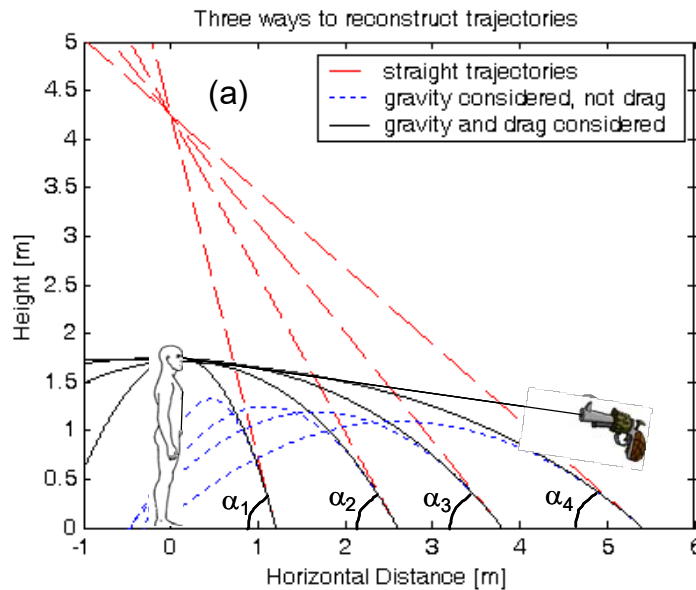


Figure 2: Illustration of the backward reconstruction of trajectories of four bloodstains using straight trajectories (in red, methods of strings or currently used in crime scene investigation software) vs. ballistic trajectories considering the influence of gravity with (in black) or without drag (in blue).

2.1.2. Inspection of stains in three dimensions

Acquisition of a digital microscope with the ability to scan bloodstains in 3D

To determine the impact conditions, the drop volume and impact speed, an innovative method of stain inspection is used. Indeed, bloodstains have always been measured in two dimensions, but stains are in fact three-dimensional objects, with a height on the order of tens of micrometer, as shown by our measurement in Figure 16.

Using a 3D microscope, with resolution of approximately 1 micrometer, we can determine the volume of a stain. This volume decreases when the bloodstain dries, but then is very stable over time for the period of interest in forensics, from 1 day to 30 days after the generation of the spatter, as per the logarithmic plot on Figure 17. The relation between stain volume and drop volume being remarkably constant [30], the drop volume can be determined. The impact velocity is inferred from the drop thickness. Note that the 3D microscope is portable to a crime scene and the the PI group is working on calibrating a pattern recognition method [31] (based on high-resolution 2D pictures) with 3D microscopy calibration images, to make the method fully compatible with current crime scene inspection practices.

The procedure to reconstruct the curved trajectories of the drops is based on the assumption that the impact conditions can be determined from the inspection of the stains. To that purpose a 3D digital microscope (Hirox KH-8700) has been acquired and modified to be portable to a crime scene. The device is transportable and able to scan bloodstains in 3D with 1-micrometer accuracy and resolution in the direction perpendicular to the stained surface. The device was acquired after a bidding and testing process that involved three vendors and two demonstrations at Iowa State University. The typical time to scan a 1x2 mm bloodstain is about 40 minutes. This corresponds to one full day of work for a skilled operator to scan the number of stains (12) typically measured in a BPA spatter for the determination of the area of origin.

Modification of a 3D digital microscope for portability to a crime scene

A boom stand was used to modify the 3D microscope and make it portable, possibly to a crime scene. Figures 3-6 show how large an area (represented by hatches) the modified 3D microscope can measure when attached to the boom stand at different views. These areas are appropriate for typical blood spatters.

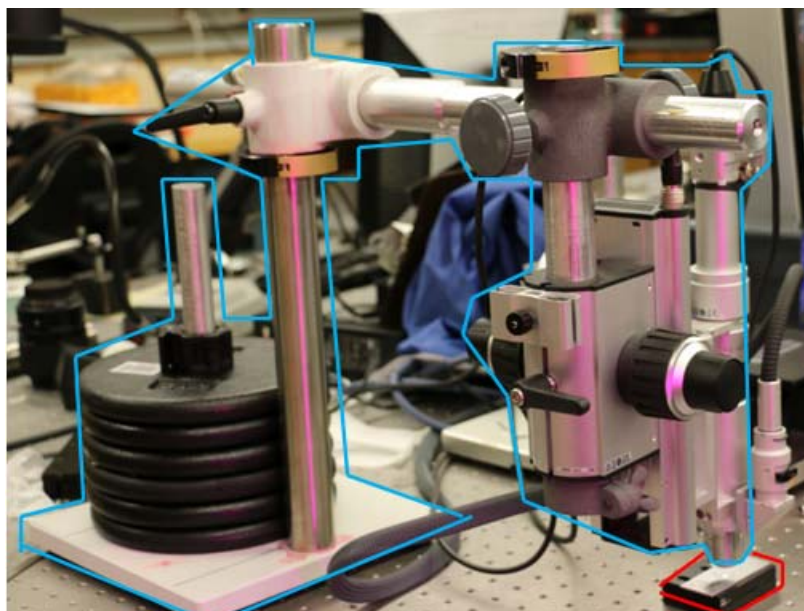


Figure 3: Experimental setup for floor scanning.
Blue=boom stand+ 3D microscope, Red= target surface

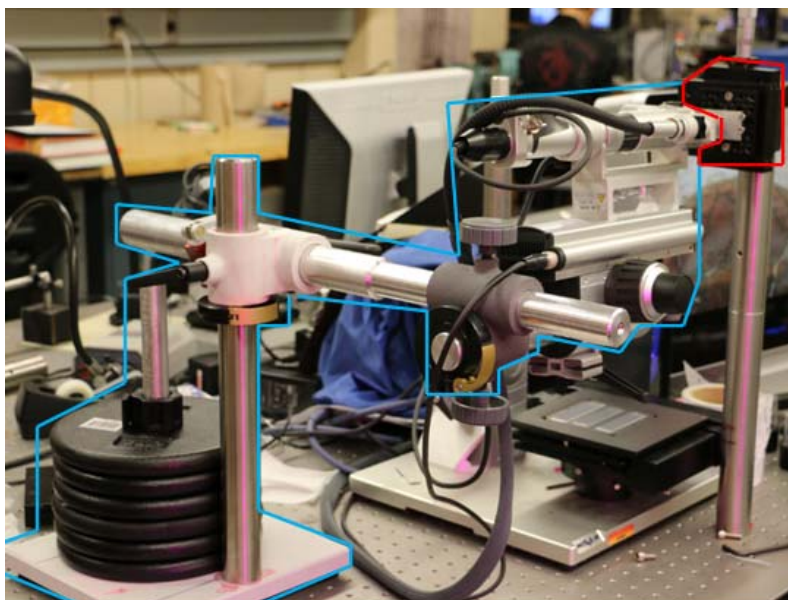


Figure 4: Experimental setup for wall scanning

Floor Scanning

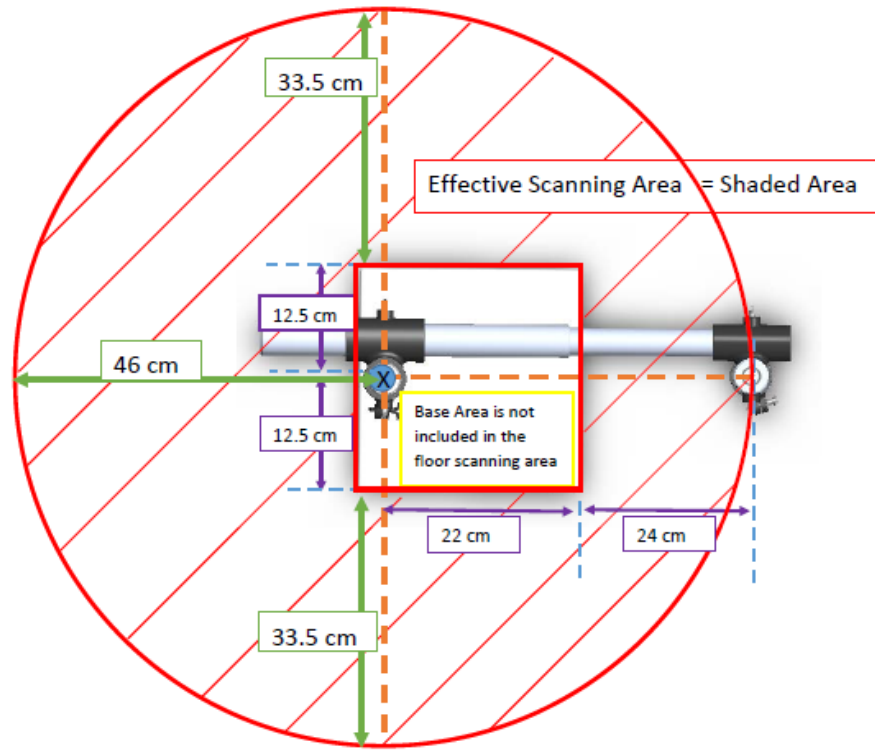


Figure 5: Top View (attached the 3D microscope to the hanging bar. The hanging bar is parallel to the vertical post with a scanning area of 360° rotation around the vertical post, excluding the base area).

Wall Scanning

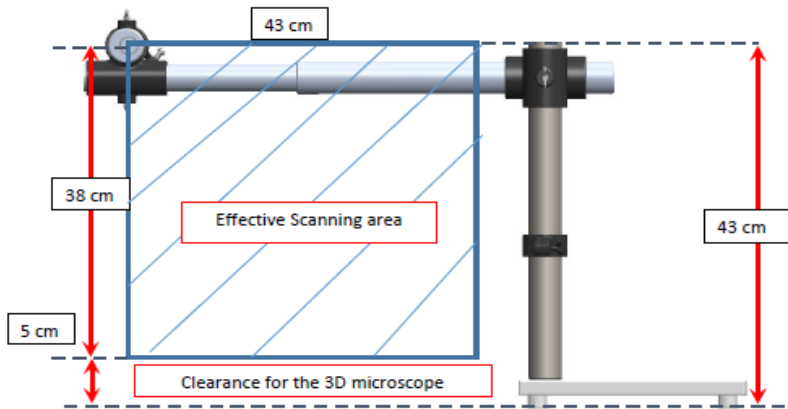


Figure 6: Side View 2 (Same as side view 1, but the horizontal arm is rotated 180° around the vertical post).

2.2. Single drop impact experiments: dripping drops

Performing measurements of impacts of dripping blood seems trivial, but it is far from simple when a complex fluid such as blood is used. Here we describe with extensive details how the impact of drops of dripping blood was measured on different substrates: glass, textured white cardstock, polycarbonate, and aluminum surfaces, which represent a range of non-absorbing surfaces. The primary objective of this study is to observe the effect of substrate roughness and contact angle on the stain diameter (or β) and, therefore, formulate substrate-specific correlations for blood droplet impact.

Several values of surface roughness for polycarbonate and aluminum surfaces are obtained after grinding with sand paper and subsequent rinsing with isopropanol and deionized water. Then, to dry the targets, the aluminum surfaces are wiped with clean tissue, while only compressed air is used for polycarbonate to prevent the formation of static charge on the surface. Surface roughness of the targets is measured using a 3D microscope (Hirox, Digital Microscope, KH-8700). The static contact angle of the blood drops, on the targets, is measured using ImageJ software [32]; the corresponding values are listed in table 1.

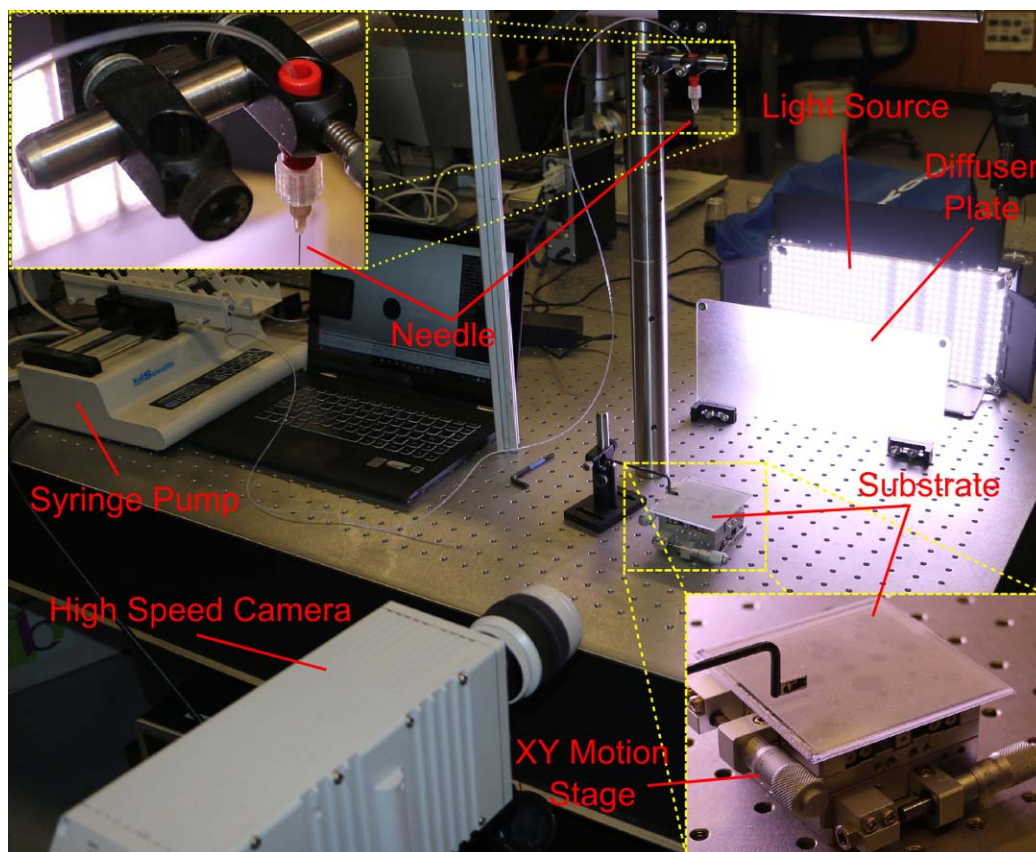


Figure 7: Experimental setup for conducting impact experiments of drops of dripping blood.

A syringe pump (KD Scientific, KDS230) is used to generate blood droplets, through FEP tubing and a 27 gauge blunt needle, as shown in Figure 7. The blood is continuously pumped (at 0.1 ml/min), without stopping, to prevent its drying at the needle outlet; drying of blood at the needle outlet has been observed to modify drop diameter over time. The corresponding dripping period is approximately 5 seconds. Droplet impact velocity is altered by changing the droplet release height (5, 10, 20, 60, and 150cm). At each change of height, the needle is replaced to ensure consistent nozzle condition. The targets are blown with compressed air just before the start of the experiments, to remove any existing dust particles. Series of 10 blood stains are generated on each surface, at each height, to ensure repeatability of results. A high speed camera (Redlake MotionXtra HG-100K) is used to record the droplet impact, while the dripping rate is kept constant. The corresponding average droplet diameter is 2.47mm. Within 70% population interval, the uncertainty on the measured droplet diameter is 3.1%, and less than 6.2% for impact velocity.

Target	Contact Angle (°)	Surface Roughness, Ra(mm)
Glass	16.1	-
Aluminum Mirror	87.1	0.32
Aluminum P600 grit	62.2	0.4
Cardstock	96.8	1.09
Bare Plastic	86.9	0.22
Plastic P20 grit	98.6	4.5

Table 2: Static contact angle of blood drops on different substrates and the surface roughness values.

2.3. Single drop impact experiments: microdrops

Two different target surfaces were chosen for the drop impact experiments: sanded aluminum and cardboard. Although there is a wide range of targets found at crime scene, these two targets are significantly different in terms of wettability. For instance, blood on cardboard has a wetting angle of $99\pm 4^\circ$, while blood on aluminum has a wetting angle of $\sim 57\pm 4^\circ$. Other categories of substrates were tested but were found to be unsuitable for BPA: glass have a very low wetting angle $20\pm 4^\circ$, and contemporary wallpaper and polymers has a very large wetting angle of $\sim 120^\circ$, and both surfaces were found to often causes drops to delaminate a few hours after drying. The average surface roughness of the sanded aluminum tiles was $3\pm 1 \mu\text{m}$. The stiffness of aluminum prevented deformations of the target due to the drying of drops, which might have added noise to the development of the measurement method involved in this study.

To select the size of the drops, we considered that the size of drops involved in BPA vary from a few micrometers (in high energy atomization events such as gunshots), to about 5 millimeters (dripping drops) as shown in Figure 8. While it is easy to generate small drops or large ones, using either inkjet printing techniques (where acoustic or volume perturbation overcome surface forces), or droppers (where gravity overcomes surface forces), the generation of drops with diameters $200\mu\text{m} < d < 2\text{mm}$ is technically difficult. This situation is problematic for BPA because drops with $200\mu\text{m} < d < 2\text{mm}$ are the ones typically involved in BPA studies towards reconstruction of curved trajectories.

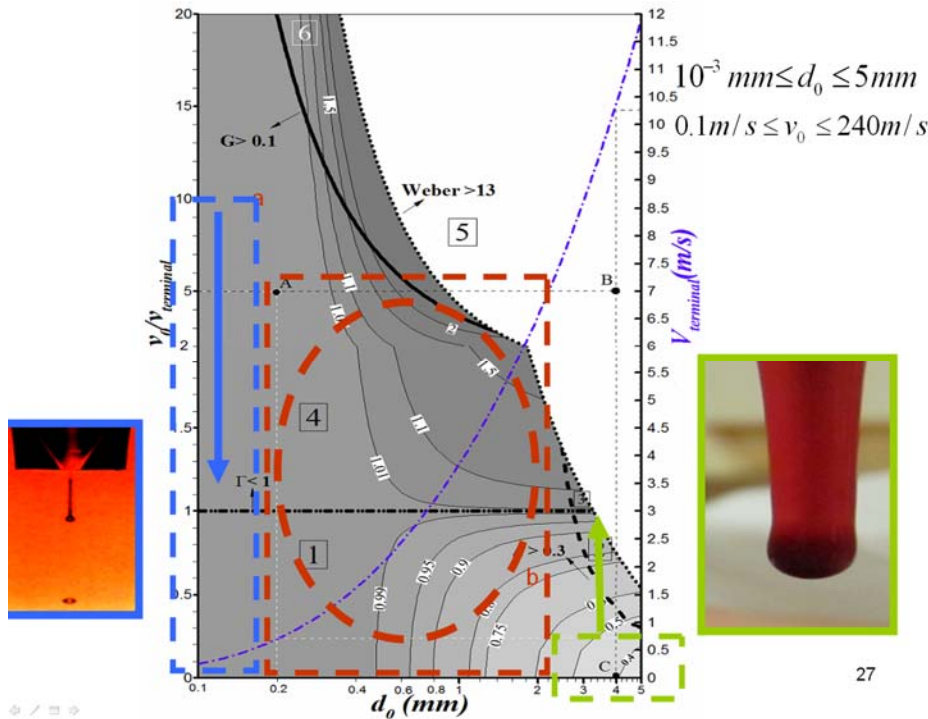


Figure 8: The grayscale plot, from [17] shows the size and velocities of drops relevant to BPA. While it is easy to generate drops in the blue and green domains, drops in the red domain, with $200\mu\text{m} < d < 2\text{mm}$ are more difficult to generate, although these are the most relevant to the problem of finding the region of origin of a blood spatter. The next figure shows the device that we developed to generate drops with $200\mu\text{m} < d < 2\text{mm}$.

To solve this issue, an experimental setup based on the pulsed atomization of a large drop and the mechanical focusing of the atomized drops has been built. A schematic of the setup used in this experimental study was shown in Figure 9. A one-mL syringe connected with syringe pump (kdScientific 780230) was used to form a $12\ \mu\text{l}$ drop on tip of 0.91mm diameter needle in front of air valve (air gun). It was shot by air gun to generate various size of drops. Camera was placed to capture drop that pass through holes of two plates placed in front of air valve. Size of holes ($d_1 = 1.5\ \text{mm}$ and $d_2 = 1\text{mm}$) and position ($X_1 = 50\text{mm}$, $X_2 = 100\text{mm}$ and $X_3 = 110\text{mm}$) of two plates (plate thickness = 1mm) from the tip of needle were designed in such way that only one blood drop passes from one shot and it should impact within range of camera field of view. A REDLAKE Redlake High-Speed Camera (motion Extra HG- 100K) was used to capture drop motion and drop impact behavior on target surface. The light was placed opposite to camera. The camera field of view, $480\ \text{pixel} \times 112\ \text{pixel}$, is suitable to capture $100\ \mu\text{m}$ to $800\ \mu\text{m}$ drop for range of velocity $1\ \text{meter per second}$ to $20\ \text{meter per second}$. Special arrangements were made in windows and target area to capture the drop impact on oblique surface. The inclination angle of the impact plate was measured precisely from the camera images with an accuracy of $\pm 1^\circ$ there is no rebound of drop observed on an aluminum surface.

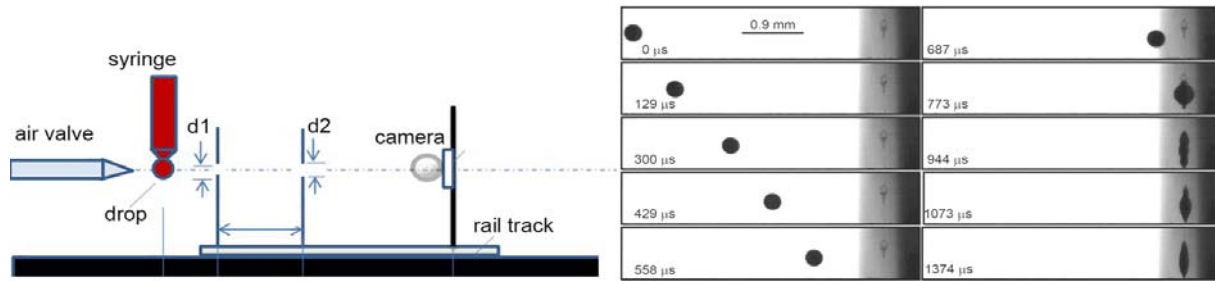


Figure 9: An experimental setup based on the pulsed atomization of a large drop and the mechanical focusing has been built in Attinger’s lab, which allows the high speed visualization of drop impact with diameters $200\mu\text{m} < d < 1\text{mm}$ and velocities between 2 and 10m/s.

The impact velocity was measured from the sequence of images. Figure 9 shows sequence of images of drop flying before the impact of drop.

The diameter of a droplet was measured from the droplet image just before impact to minimize the error due to evaporation of drop during the flight. As stated previously, drop rotate own center of mass during flying and the shape of drop shape was not perfect spherical. It was observed that the diameter of drop parallel to the direction of motion is higher than the diameter perpendicular to direction of motion. Both parallel and perpendicular diameter were measured. The equivalent drop diameter is as:

$$D_d = (D_{\parallel} \times D_{\perp}^2)^{1/3} \quad (3)$$

Where D_d is diameter of drop, D_{\parallel} is the parallel diameter drop in direction of motion and D_{\perp} is the diameter of drop in perpendicular the direction of motion, was calculated assuming that the droplet is rotationally symmetric with respect to the perpendicular the direction of motion.

A 3D microscope (Hirox, digital microscope KH-8700) was used to measure the volume, width and length of the stains. Stains are dried up to 12 hours before scanning with 3D microscope.

The ratio β of stain characteristic diameter (D_s) to drop diameter (D_d), is correlated with the dimensionless number $Re^2 Oh$. Here Re is the Reynolds number and Oh is Ohnesorge number. These number are defined as:

$$Re = \frac{\rho D_d U_n}{\eta} \quad (5)$$

$$Oh = \frac{\eta}{\sqrt{\rho D_d \sigma}} = \frac{\sqrt{We}}{Re} \quad (6)$$

In addition, the ratio of drop stain volume (V_s) to drop volume (V_d), ($\beta_1 = V_s/V_d$) were also measured.

2.4. Blood spatter experiments

Here, we report a set of four experiments with a modified mousetrap to produce spatters from known region of origin. There are several reasons for using a mousetrap: by creating a sheat that breaks into threads and then drops, the device models the generation of impact spatter stains, with the appropriate range of drop sizes and velocities. Also, since the spatter is created from a

flat rather than crown-like blood sheet (because of the planar nature of the trap), it produces spatters that do not typically exhibit a radial nature – which makes the determination of the region of origin almost impossible using state of the art techniques. The horizontal distance between the wall and the region of origin has been varied from 50cm to 200cm – which is very large for BPA. To facilitate the inspection of stains with the three-dimensional microscope described in section 3.2.1, the spatters were produced on a collection of 5x5cm aluminum tiles screwed onto a wood board. The stains were sanded with 600 grit sandpaper and had an average roughness below 3 micrometer.

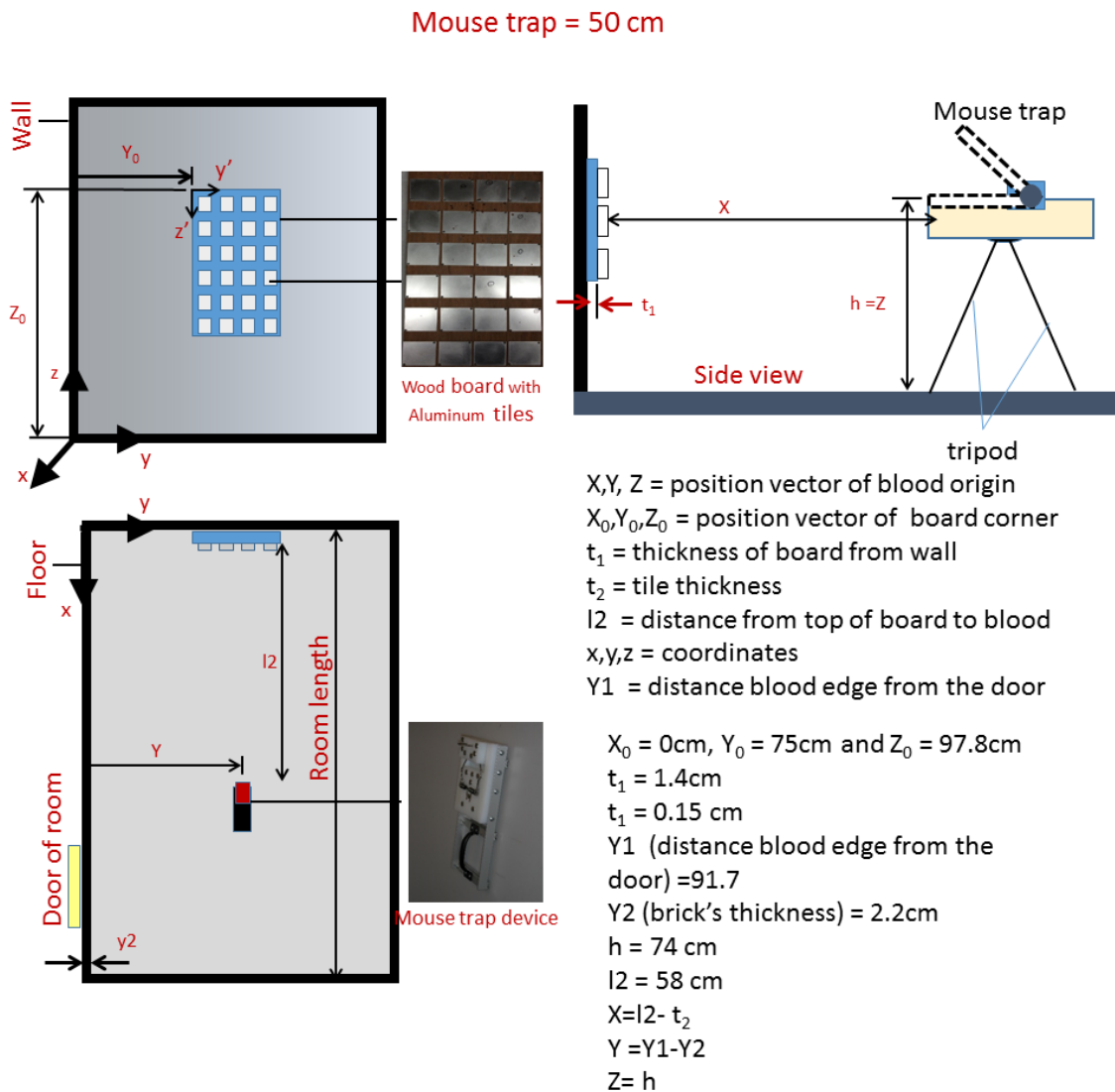


Figure 10: Setup of the blood spatter experiments, using a mousetrap to generate spatters analog to beating events.

2.5. Measurement of the physical properties of blood

Pig's blood rather than human blood was used throughout this study, for two reasons: It is an accepted blood substitute because it has similar viscosity, surface tension, shear-thinning behavior as human blood[5], and to drastically reduce the chances of contamination to the researchers, and significant safety concern in a university environment, –BPA research being sometimes difficult to fully control, as in studies involving the generation of impact spatters.

2.5.1. Rheology (*shear viscosity*)

The *shear viscosity* of blood has been measured with state-of-the art rheometers, according to the following procedure. Several vials of the same blood, spiked with anticoagulant (1 vol% heparin), were placed in a warm water bath for 1 hour under light agitation, and then mixed in a larger beaker. Once the blood reached room temperature, its hematocrit was measured. The flow curves (the stress-strain rate relations) in simple-shear flow were measured using a LV-II+ cone and plate Brookfield viscometer. During each trial the sample temperature was kept constant by the temperature-control system of the viscometer. The shear rate was first raised by equal increments. After reaching the maximum, the shear rate was decreased by the same increments back to the initial value. Each shear rate was maintained for 30 seconds. The readings were done moments before a speed change. Three types of protocols of measurements in the simple-shear flow were used. The first was for the shear rates in the range 7 s^{-1} to 350 s^{-1} using spindle SP 40. The second one was for the shear rates in the range 200 s^{-1} to 400 s^{-1} using spindle SP 52. The third protocol covered the low shear rates in the range 7 s^{-1} to 60 s^{-1} using spindle SP 40.

2.5.2. *Equilibrium surface tension of blood*

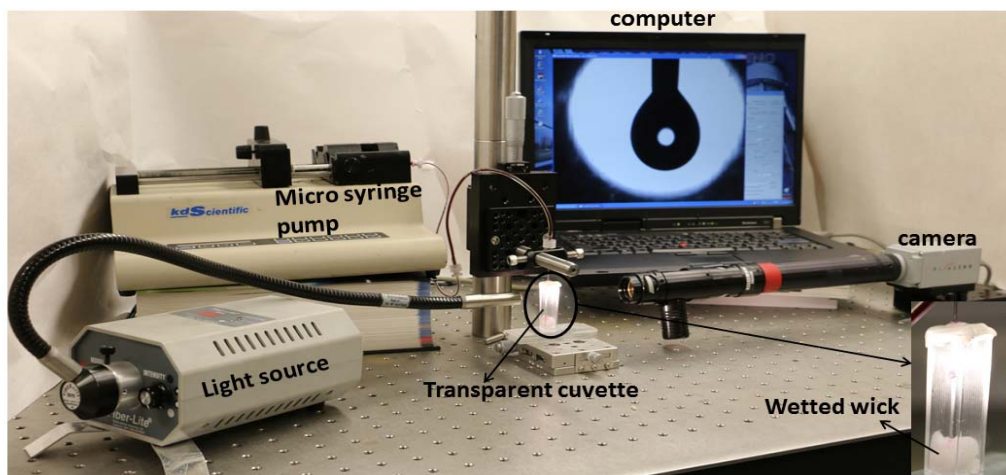


Figure 11. Photograph of the pendant-drop experimental setup to determine surface tension.

The *equilibrium surface tension* of blood was measured as follows. The experimental setup depicted in Figure 11 was used to capture images of a pendant drop of blood. The setup consists of a cubical transparent chamber (1 cm x 1 cm x 4 cm), which is about twice as large as the drop diameter. It contains a wet piece of cotton to moderate evaporation by maintaining a high humidity level. A syringe pump supplied a given volume of liquid ($\sim 8 \mu\text{L}$) to form a pendant drop at the tip of a vertical 20 gauge blunt needle. The image of the pendant drop was captured using a digital camera. A diffuser between the light source and the drop ensured a sharp contour of the drop. The pendant drop method^[33] was then used to determine the equilibrium surface tension of blood. The method is based on optimizing the numerical approximation of the measured contour of a pendant drop by a theoretically predicted one (based on a numerical solution of the Young-Laplace equation) with the surface tension being a fitting parameter.

2.5.3. *Hematocrit measurement*

The blood hematocrit was measured with a centrifugation device (HemataSTAT® II). The technique requires that the capillary blood tubes be centrifuged at 12000 rpm for one minute. For convenience and ease of use, the HemataSTAT-II machine also includes a built-in automatic tube reader.

2.6. **Low-cost measurement of shear viscosity and equilibrium surface tension**

The measurements described in section 2.5 are accurate but based on state-of-the art devices costing between \$10K and \$300K. To encourage all the BPA research groups to measure the properties of the blood used in their studies, we have also developed two cheaper instruments which measure the shear viscosity and the equilibrium surface tension of blood. These instruments are described in Figure 12, with their operating principle, the range of physical properties that can be measured, an estimation of the root mean square (RMS) uncertainty, and a picture of the existing setup.

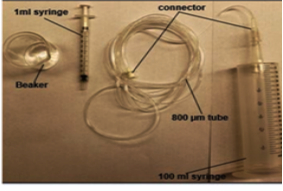
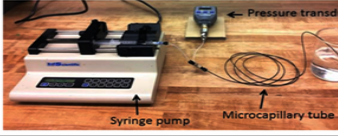
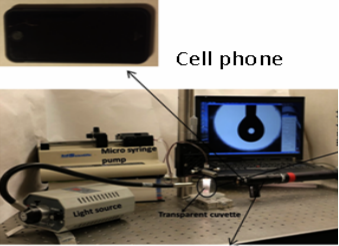
Name of equipment	Physical property and range	Cost (USD)	Sources of error	RMS uncertainty (%)	Image of setup
Gravity-driven micro-capillary viscometer	Viscosity $5 < \eta < 10$ (mPas) $60 < \dot{\gamma}_{non-N} < 500$	80	$(\Delta\eta/\eta)_1 = 3\%$, $\Delta T = 1K$ $(\Delta\eta/\eta)_H = 1\%$, $\Delta H = 1cm$ $(\Delta\eta/\eta)_V = 3.5\%$, $\Delta V = 0.1ml$ $(\Delta\eta/\eta)_t = 2\%$, $\Delta t = 2sec$	5%	
Syringe pump driven micro-capillary viscometer	Viscosity $3 < \eta < 20$ (mPas) $10 < \dot{\gamma}_{non-N} < 1200$	2300	$(\Delta\eta/\eta)_1 = 3\%$, $\Delta T = 1K$ $(\Delta\eta/\eta)_P = 3\%$, $\Delta P = 0.1$ inHg	4%	
Pendant drop method for surface tension measurement (typical cell phone of 13Mpixel)	Surface tension $20 < \gamma < 72$ (mN/m)	60	$(\Delta\gamma/\gamma)_T = 2\%$, $\Delta T = 1K$ $(\Delta\gamma/\gamma)_D = 4\%$, $\Delta D = 25\mu m$ $(\Delta\gamma/\gamma)_d = 4\%$, $\Delta d = 25\mu m$	5%	
Pendant drop method for surface tension measurement (Canon 70D, resolution = 2μm)	Surface tension $20 < \gamma < 72$ (mN/m)	1800	$(\Delta\gamma/\gamma)_T = 2\%$, $\Delta T = 1K$ $(\Delta\gamma/\gamma)_D = 4\%$, $\Delta D = 2\mu m$ $(\Delta\gamma/\gamma)_d = 4\%$, $\Delta d = 2\mu m$	2%	

Figure 12: Description of four experimental tools developed during this project to measure the physical properties of blood: the top two instruments measure shear viscosity, and the bottom two measure surface tension.

The capillary viscometer measures the pressure drop along a thin tube under a given flow rate [34]. The gravity-driven micro-capillary viscometer determines the shear viscosity of an incompressible fluid by measuring an internal steady-state flow in a thin tube [33]. The raw data for capillary viscometer measurements are the pressure and volumetric flow rate. The micro-capillary tube viscometer used in this study was designed to measure the shear viscosity of blood on the base of a power-law model coupled with the Rabinowitch-Mooney (RM) equation, as described in [33, 34],

$$\dot{\gamma} = -\frac{Q}{\pi R^3} \left(3 + \frac{d \log Q}{d \log \Delta P} \right), \quad (7)$$

$$\text{where } n = \frac{d \log \Delta P}{d \log Q}. \quad (8)$$

In the above equations, ΔP is the pressure difference, R is the internal radius of the tube and L is its length. The non-Newtonian viscosity μ can then be found with as $\tau_{shear} = K(\dot{\gamma})^n$, where τ_{shear} is the shear stress, $\dot{\gamma}$ is the non-Newtonian shear rate, and K and n are the consistency and flow behavior indexes, respectively. The non-Newtonian viscosity was measured over a representative range of shear rates (10 to 1000 per second).

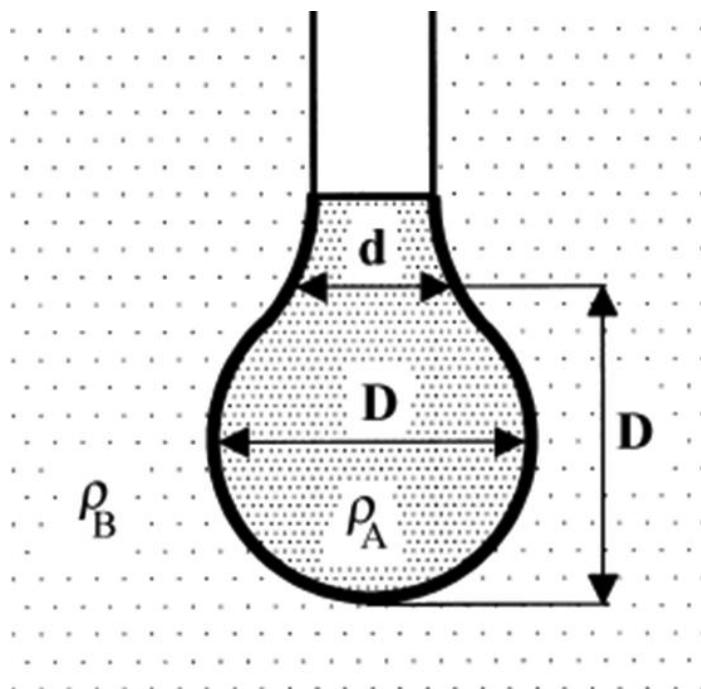


Figure 13: Schematic illustration of two diameters measurement of pendant drop for measuring surface tension

The pendant drop method determines the equilibrium surface tension from the shape of a pendant drop, which is controlled by the balance of gravity and surface tension forces [35]. These designs and devices have been presented at a fluids engineering conference [36, 37]. The gravity driven viscometer and pendant drop method are both portable devices that could both be offered at a cost below \$200, or assembled at a similar cost, so that these devices would measure physical properties within $\pm 5\%$ RMS uncertainty, at a cost affordable for any BPA research group. To determine the equilibrium surface tension of the blood, the pendant drop technique that reported by Stauffer [38] was used to determine surface tension of blood. This method is well established and highly accurate (0.1mN/m). Only two parameters of the pendant drop are measured: the equatorial diameter D and the diameter d at distance D from the apex of the drop, as shown in Figure 13. The basic recommendation for this technique is that needles with a diameter that is less than $0.5D$ be used.

These methods have been presented at a Fluids Engineering conference [37], and submitted as journal articles [39, 40].

2.7. Wettability measurements

Wettability measurements were made with an in-house goniometer. Substrates were prepared by sanding and inspected with a 3D microscope to measure the average and peak roughness.

2.8. A numerical simulation tool to simulate blood drop impacts

A subaward to Dr. Adam Donaldson at Dalhousie University has been used to develop and validate an open-source CFD code for simulating blood spatter impact on target with different wettabilities (e.g. cardstock or metal). The intent of the work is to provide a framework by which practicing forensic scientists could explore different impact conditions and scenarios to better understand the spreading process and to offer a tool that allows for the visualization of impact under conditions that are difficult to recreate experimentally. Sometimes also, it is interesting to investigate the effect of a single variable that would be difficult to vary experimentally, such as the substrate wettability, the substrate temperature, or the ambient humidity. The resulting model was validated against experimental data provided by Dr. Attinger for pig blood under a variety of impact conditions. Results from an earlier version of this CFD model were initially published in Forensic Science International as part of a larger review of BPA as a field, and the most recent results are currently being prepared for publication in a series of papers looking at the model's validation and application to BPA, and its application to oblique impact conditions. The following summary provides a description of the most recent state of this work, including excerpts from the current draft publications. The open source code could be used for teaching, planning experiments, and assisting court cases.

3. Results and Discussion

3.1. Reconstruction of curved trajectories of blood drops from stain inspection in blood spatter

A set of experiments of backward trajectory reconstruction was done using the above numerical method, with a horizontal distance varied between .5 and 2 meter between a mousetrap and the impact region. Our results in Figure 14 and Figure 15 show the large errors associated with the assumption of straight trajectories. The mousetrap experiments described in section 2 produce a spatter with velocities and drop size characteristic of a beating event. Like all laboratory experiments, it is important to understand that that the situation in a crime scene can be more complex and not fully known (motion of the blood source during atomization, mechanical compliance of the surfaces where blood originates from). The correlation used to determine the impact conditions from 3D stain inspection is that determined in section 3.4.

In the figures below, the curves are obtained as follows, from their impact conditions on the target at $X=0$ (impact velocity, angle and position). The red curves are obtained assuming that the blood travels in straight lines, as is done with state of the art techniques currently used in BPA in 2015 (e.g. method of strings or Hemospat software). The blue curves are obtained by assuming that gravity modifies the trajectories, neglecting the influence of aerodynamic drag. The blue curves are obtained by assuming that gravity and drag modifies the trajectories, as per the framework described in section 2.1.1.

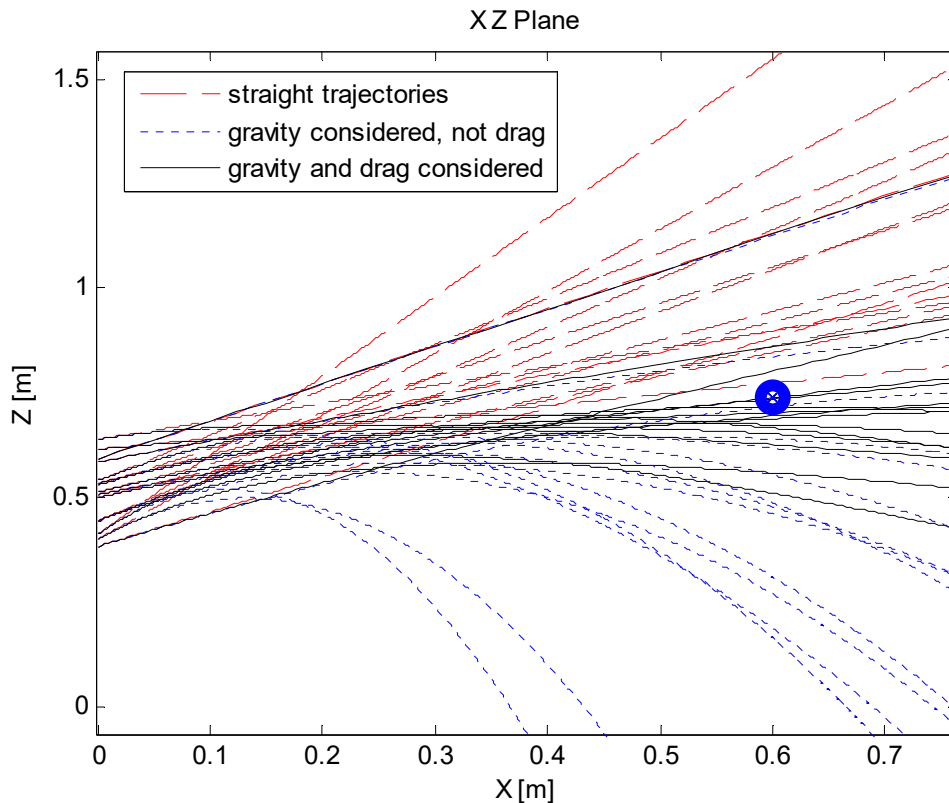


Figure 14: Reconstruction of backward trajectories (red=method of strings, blue=curved trajectories considering gravity, black=curved trajectories considering drag and gravity). The experiment is realized with pig's blood under conditions of known region of origin (in that case, the mousetrap, pictured as a blue circle, was 62cm away from a vertical wall, left (hematocrit is 42%, $T=25C$). The consideration of gravity and drag forces increases the accuracy of the determination of the region of origin.

The results shown in the figure below show that the backward reconstruction of trajectories improves the determination of the region of origin by about 4 times for this specific set of representative experiments. Three observations are important. First, all the stains measured are pointing downwards, by design of experiment. Second, the straight trajectories (which correspond to the state of the art in BPA) overestimate the height of the point of origin, which makes sense, because the deflection of the trajectories by gravity is not accounted for. Third, the consideration of gravity without drag significantly underestimates the height of the region of

origin. This seems counterintuitive, however when reconstructing the trajectories backwards, neglecting drag increases the travel time, thus the effect of gravity.,

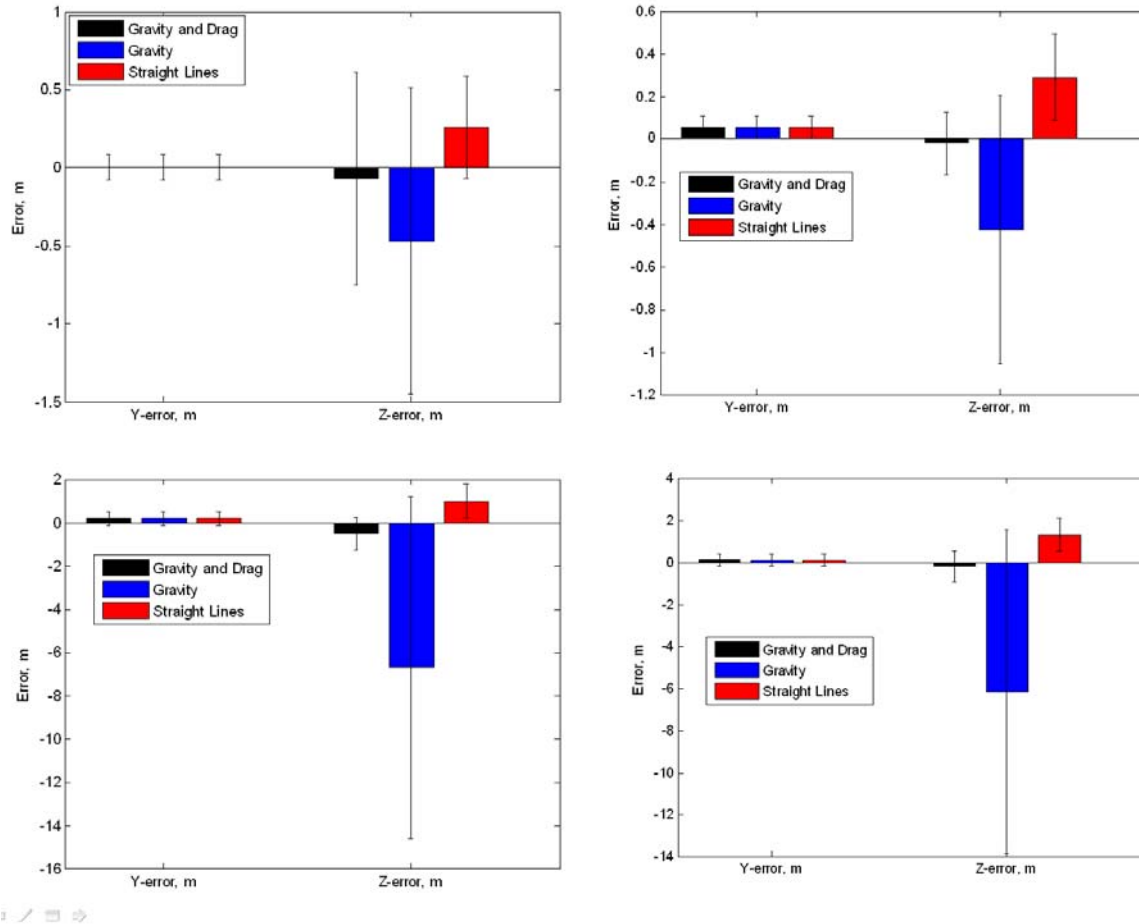


Figure 15: error in the determination of the height of the region of origin of four blood spatters, using pig’s blood at ambient temperature (hematocrit is 42%). Three different methods are compared (red=method of strings, blue=curved trajectories considering gravity, black=curved trajectories considering drag and gravity) for backward reconstruction of the trajectories. The horizontal distance between the vertical impact wall and the mousetrap was 60cm for the above two cases and 2m for the bottom two cases.

3.2. Determination of impact conditions from stain inspection

3.2.1. Inspection of stains in three dimensions.

Example of bloodstain scanned in 3D is shown in Figure 16. The purpose of scanning bloodstains in 3D is related to the need to determine impact velocity and droplet size to reconstruct curved trajectories. The graph on the right of Figure 16 shows that the noise (seen by the measurement of the flat surface) is at least one order of magnitude of the ring height (180 micrometer for that stain).

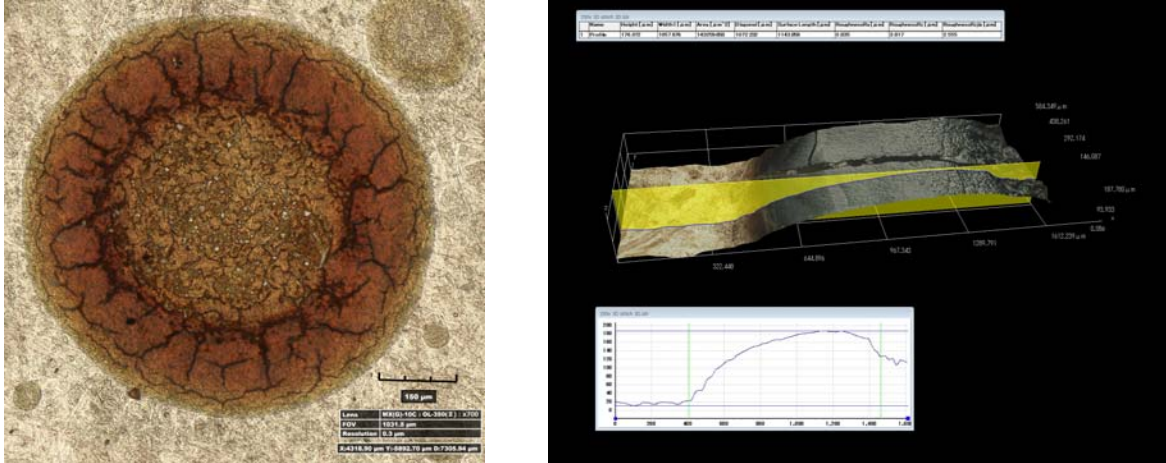


Figure 16: Examples of 3D scan of bloodstains dried on an aluminum surface. (full view and detail of the peripheral ring). Units on the graph are in micrometer.

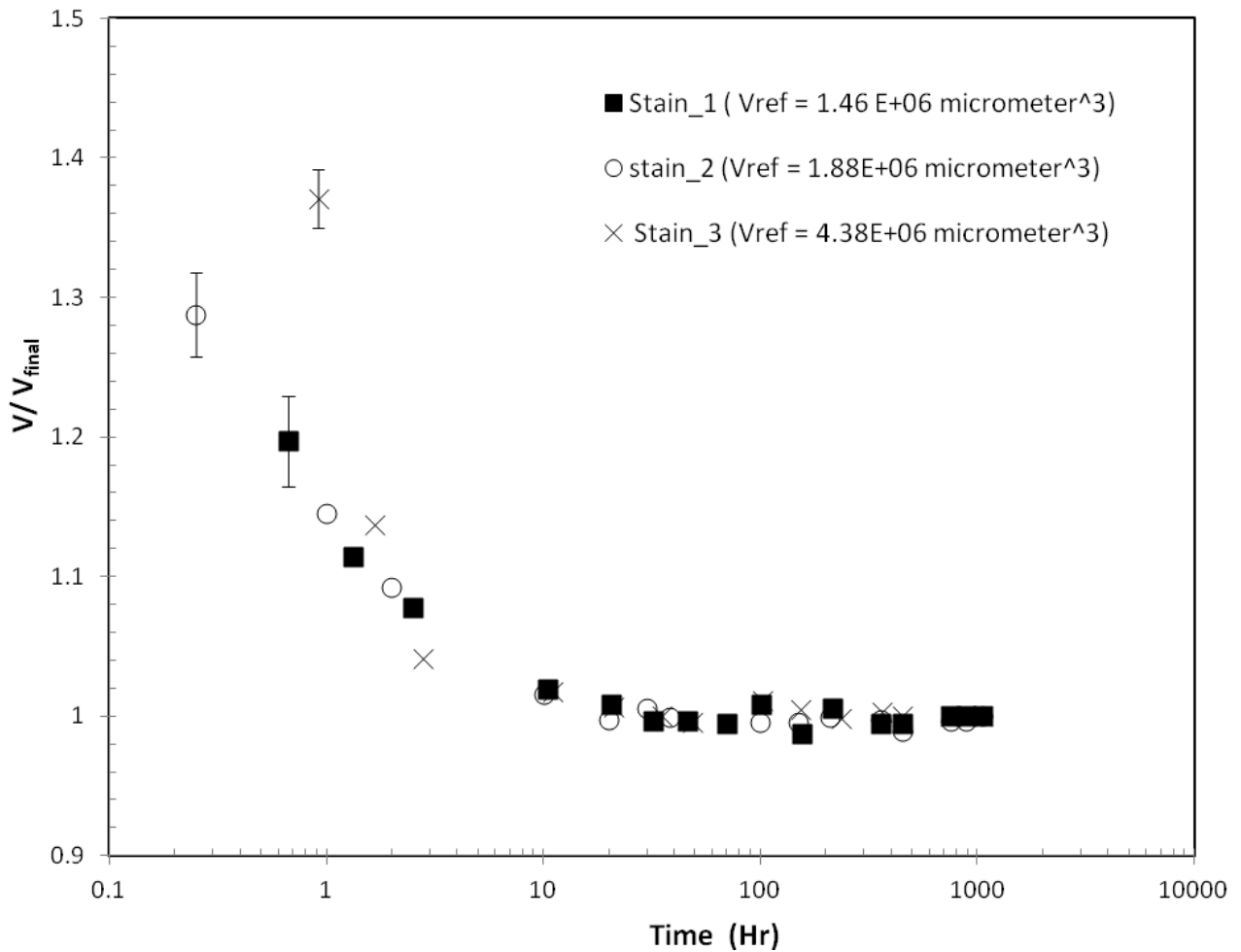


Figure 17: Evolution of the volume (V/V_{ref}) of stains with respect to drying time. Pig's blood with a hematocrit of 42% is used in this case.

During the drying process, the stains volume decreases. The decay stains depends on several factors such as temperature, relative humidity, percentage of hematocrit, volume and thickness of stains. It is a hypothesis that the certain period of time from formation of to after the complete drying of stain, there has not been decay of volume in the stain. To verify this hypothesis, stains were formed by impact of blood drop on vertical surface. Among these stains, three stains of various sizes were chosen. These stains were scanned by three-dimension microscope at specific interval of time for measuring the volume. The measurement in Figure 17 shows that stains have a stable volume from the day after a crime for about several weeks.

3.2.2. *Comparison between stationary and portable 3D microscope*

The results of both wall and floor scanning when the 3D microscope attached to the boom stand were almost identical compare to the lab-based results when the 3D microscope attached to the Hirox's stand. Figures 18-19 show that the 3D profile of a typical stain with three different scanning methods (the Hirox stand, wall scanning with boom stand and floor scanning with boom stand) at the same location.

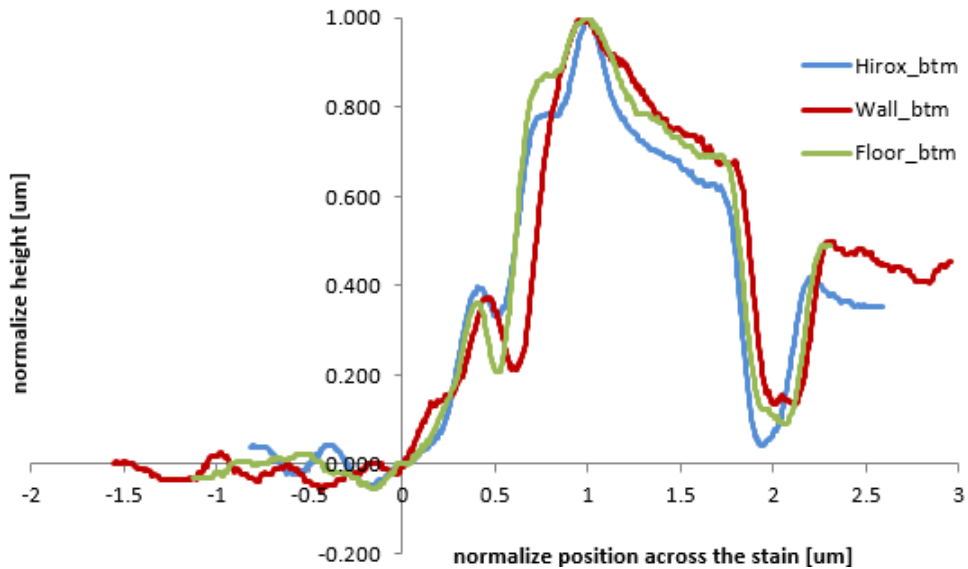


Figure 18: 3D profile using 3D scans at the bottom of stain (#N_13) by three different methods (the Hirox stand, wall scanning with boom stand and floor scanning with boom stand)

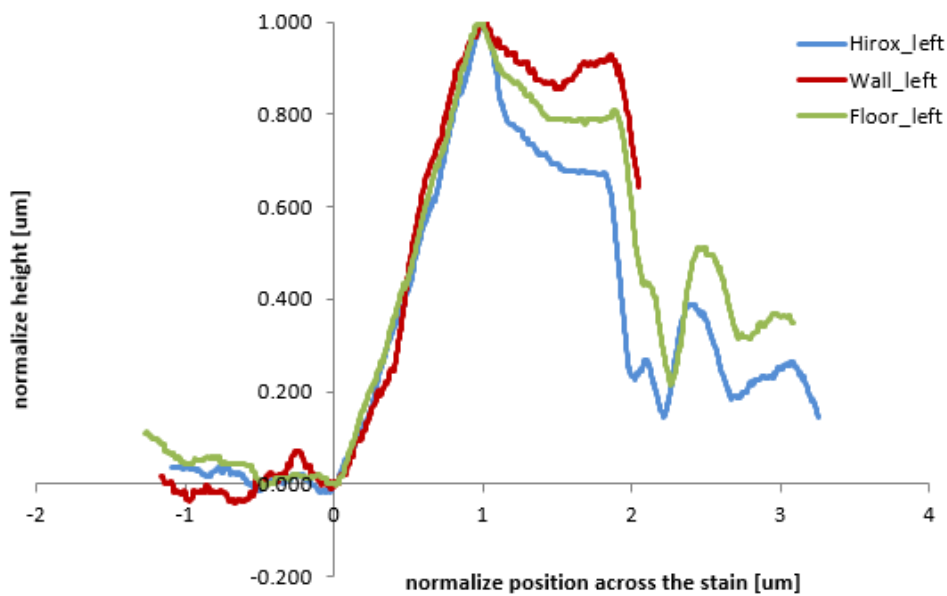


Figure 19: 3D profile using 3D scans on the left side of stain (#N_13) by three different methods (the Hirox stand, wall scanning with boom stand and floor scanning with boom stand)

. Discussion:

Stains maintain a constant volume once dried. The 3D microscope has been modified to be portable to a crime scene.

3.3. Measurement of the physical properties of blood

These findings have been submitted to a physics journal [40].

3.3.1. Rheology of blood (shear viscosity)

With collaborator Alex Yarin at the University of Illinois in Chicago, we have measured the shear viscosity of pig's blood (hematocrit 49%).

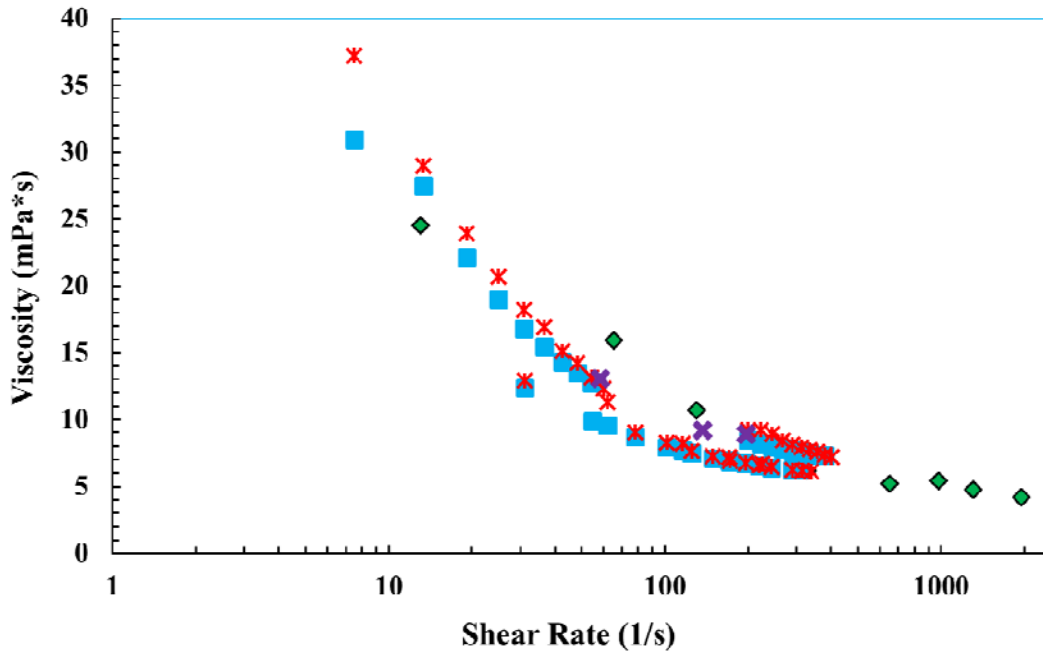


Figure 20. Shear viscosity versus shear rate in simple shear flow. The experimental data shown by diamonds was measured using a capillary viscometer driven by a syringe pump. Data shown by “x” was measured using a capillary viscometer driven by gravity. The data shown by the red asterisks (for ramp up) and blue squares (for ramp down) were measured with rotational viscometer. Pig’s blood with 29% hematocrit is used in this

In the measurements with the low-cost capillary viscometer, the flow rate ranges from 0.01 to 2mL/min, with $Re < 600$ so the flow is laminar. The flow is also fully developed, with a negligible entry length with respect to the tube length ($Le < 0.01 L$), calculated as $Le = f(n, Re)$ as per [41]. The relative uncertainty (SD = 4%) on the viscosity measurements with the capillary viscometer is due to the uncertainty on the temperature and on the pressure measurement.

3.3.2. Static surface tension of blood

For pig’s blood with 49% hematocrit, comparison between the reconstructed and observed drop shape, the static surface tension of blood was determined by the pendent drop method as shown in Figure 21, as 61 ± 2 mN/m. The simpler method to determine the surface tension of the blood measured 60 ± 2.5 mN/m.

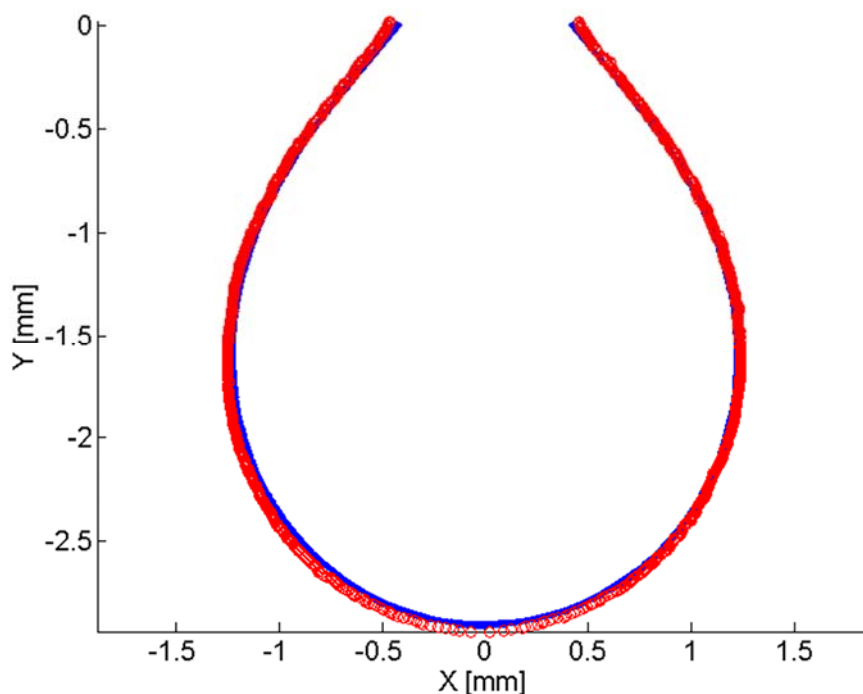


Figure 21. Surface tension measurement by the pendant drop method: circles show the experimentally measured drop contour, and the best theoretical fit with the surface tension as a fitting parameter is shown by the blue line.

3.3.3. Hematocrit measurement

Pig's blood was supplied from healthy pigs at the College of Veterinary Medicine at Iowa State University. The hematocrit was systematically measured and found to be vary between 34 and 49%., and is indicated with the several measurements described in this report.

3.3.4. Wettability Measurements

The wettability of blood was measured on two typical surfaces: sanded aluminum tiles and cardboard.

Measurement on an aluminum surface
Room temperature 26°C and RH 57.9%
Bleeding date: 18 August at 8AM
Date of experiment: 18 August at 11:00AM

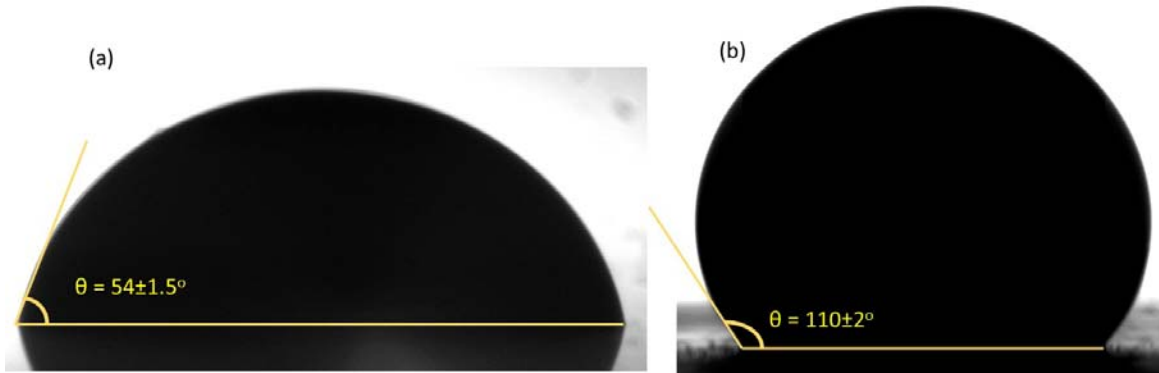


Figure 22: Wettability of blood on various surfaces (a) aluminum surface (sanding 600 grit) and (b) cardstock paper. Hematocrit of blood is as: $42 \pm 1\%$

3.4. Drop impact experiments: dripping drops

In vertical droplet impact experiment setup, blood droplet generated from a 27-gauge needle and falls onto a solid substrate from different height resulting in different impact velocity. In this experiment, the effect of the characteristics of the substrate and hematocrit on the ratio of stain diameter to drop diameter was investigated.

The representative sequence of events during droplet impact and spreading on different targets is shown in Figure 23. When the droplet impacts normally on the surface, its inertia drives the liquid radially outwards, and this expansion is opposed by viscous dissipation in the blood and by surface tension at the blood-air interface. The impact creates a lamella of the liquid in contact with the target, while the rest of the liquid spreads radially in the form of a rim. About 2-3 ms after the impact, as the inertial forces weaken, the droplet reaches a maximum spreading, whereafter capillary and viscous forces dominate. The material in the rim flows into the bulk, until equilibrium is attained, while the contact line remains pinned to the target [12, 42, 43], except on glass. As observed in Figure 23, after the instance of maximum spreading (image (iv) in figure 23), while the contact line remains pinned for the aluminium, cardstock and plastic targets, the contact line on the glass target spreads further; this is attributed to the significantly higher wettability of the glass target, due to low contact angle and roughness, compared to the other targets.

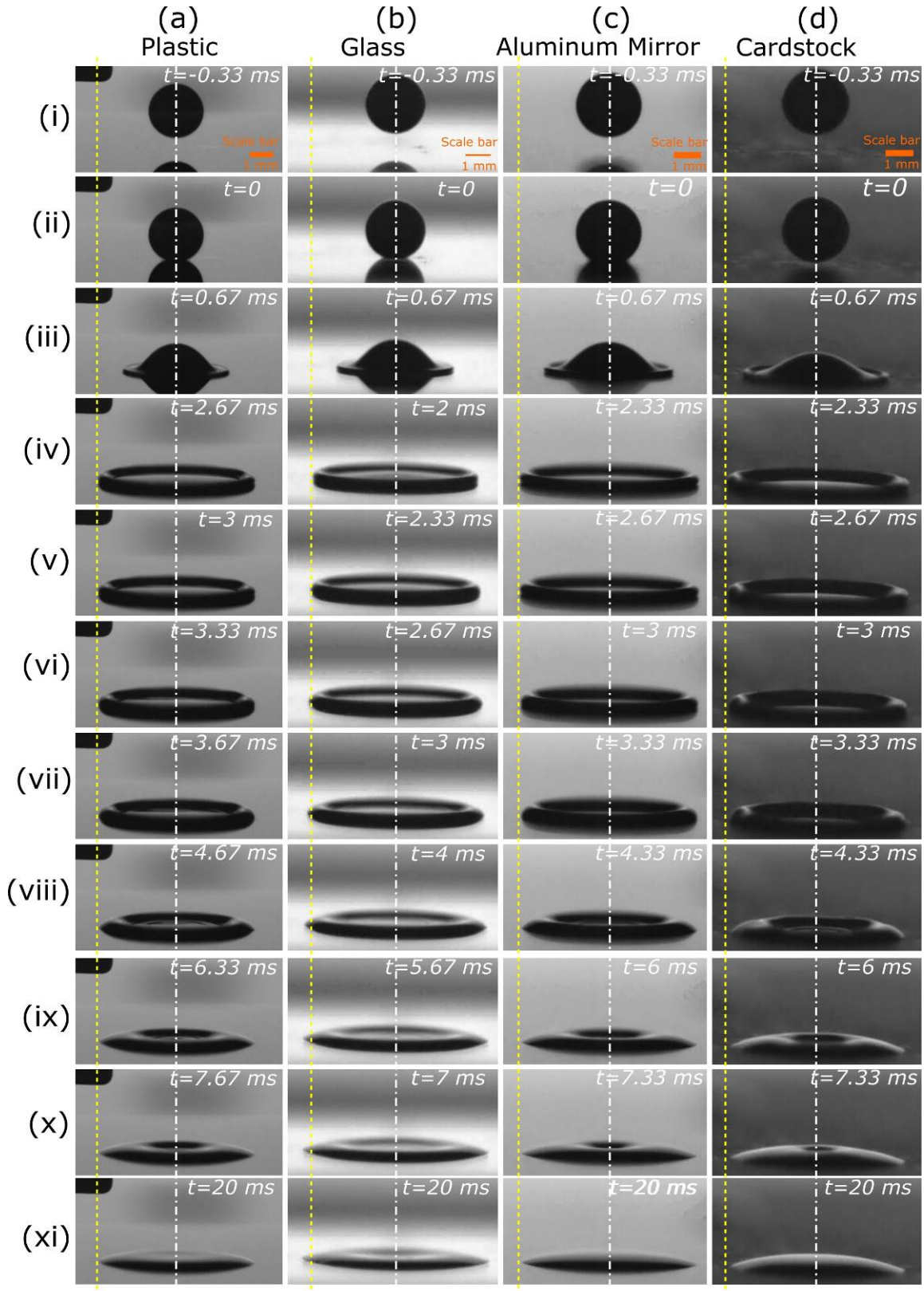


Figure 23: Evolution of blood drop spreading on different targets. (a) Bare Plastic, (b) Glass, (c) Aluminum, (d) Cardstock. The yellow lines represent the maximum extent of the spreading of the rim. The white lines represent the center of the droplet.

The droplet's impact velocity (V_i) is measured by considering the difference in height of the center of the droplets (Δs) between two frames just before the impact of the drop, and calculated as:

$$V_i = \frac{\Delta s}{\Delta t'} \quad (9)$$

where, $\Delta t'$ is the time difference between the two frames. After the impact, the droplets are left for drying (for about 24 hrs), and the diameter of the dried stain (D_s) is measured to calculate the spreading factor (β).

It is noteworthy to mention here that the dried stain diameter is observed to be approximately 2-3% smaller than the blood stain diameter after 20 ms of impact, for all the targets used in the experiments. Having obtained the spreading factor, the impact velocity and diameter, we can fit Bousfield-Scheller correlations[18] on each dataset related to a specific target, to characterize the spreading as a function of the impact conditions.

Inspection of Figure 23 reveals first how much larger the spreading is on the glass target. At low impact velocities, the spread factor on glass is on average 25% larger than on the other targets. This might be due to enhanced wetting on the glass, which has a significantly lower contact angle than other targets. As the Ohnesorge number increases, i.e. as the ratio of impact energy versus the work of resistance forces increases, the spread factor on the glass target becomes comparable with that on other targets, owing to the decreased influence of wetting forces on spreading[6].

Figure 23 also demonstrates how spreading is influenced by the roughness, for a given surface. The spreading factor for the roughened aluminum and plastic target are lower than for their respective unaltered counterparts. These observations are coherent with the observations in Patil et al. [44] and Hulse-Smith et al [12], where an increase in the surface roughness reduced spreading upon drop impact. The associated formation of spines observed in [12] is attributed to the Rayleigh-Taylor instability, which is encountered when a liquid-air interface is subjected to a sudden acceleration[12, 45].

3.5. Drop impact experiments: microdrops

Figures 24-25 show the sequence of image of drop impact on an inclined surface. In oblique impact, the shape of stains is close to elliptical. The lateral spreading (the minor axis of the elliptic stain) is driven not by whole velocity, but by the velocity component normal to the surface. The equivalent diameter based on the stain area correlates with the Re and We number characterizing the drop impact. The normal and oblique impact of swine blood drops on aluminum substrates were visualized to measure velocity of impact, diameter of impact drop and maximum spreading diameter after impacting on aluminum substrate. The primary goal of this measurement is to correlate the ratio of maximum spreading diameter to drop diameter ($\beta = D_s/D_d$) with dimensionless characterizing group ($Re^2 Oh$).

Pig blood was used for all experiments in this section, using 1% heparin heparin as the anticoagulant. The hematocrit was 42 ± 1 %. The blood static contact angle on the finished aluminum surface was $15 \pm 1^\circ$. The surface tension was measured using the pendant drop method (J. Drelich, 2002). This method gives a statistical value $0.52 \pm 0.3 \text{ Nm}^{-1}$ over 20 drops. shear rate of blood,; surface tension, 52mN/m. The viscosity was 0.003Pas at a shear rate of $1 \times 10^4 - 9 \times 10^4$ per second; drop diameter, 200-900 micrometer; impact velocity, 0.5-11 m/s; Reynolds number, 110-980; and Weber number, 15-400. The maximum error calculation in of diameter of drop and velocity is 4%, the maximum error in dimensionless maximum spreading diameter is less than 5%.

Image J (online free image processing software) was used to analyze videos to determine diameter and velocity of impact drop. The length scales on the video screen were calibrated to the actual length scales from images of a ruler held at field view of camera. The video camera viewed the impact from an angle a few degrees (2°) from the impact plane to allow viewing of the plane into the screen and to improve resolution of impact. The figure below shows sequence of image of drop normal impact on surface the video recording rate 23295 frames/s at the resolution 480 pixel \times 112pixel.

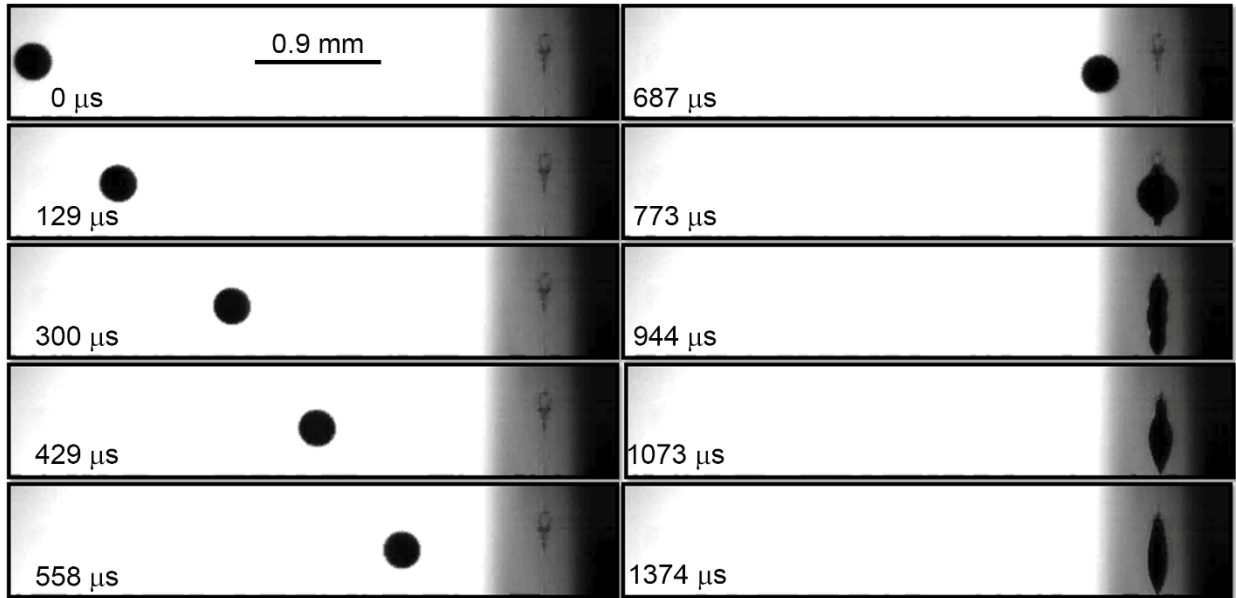


Figure 24: Sequence of images from drop flight to impact onto normal aluminum surface.

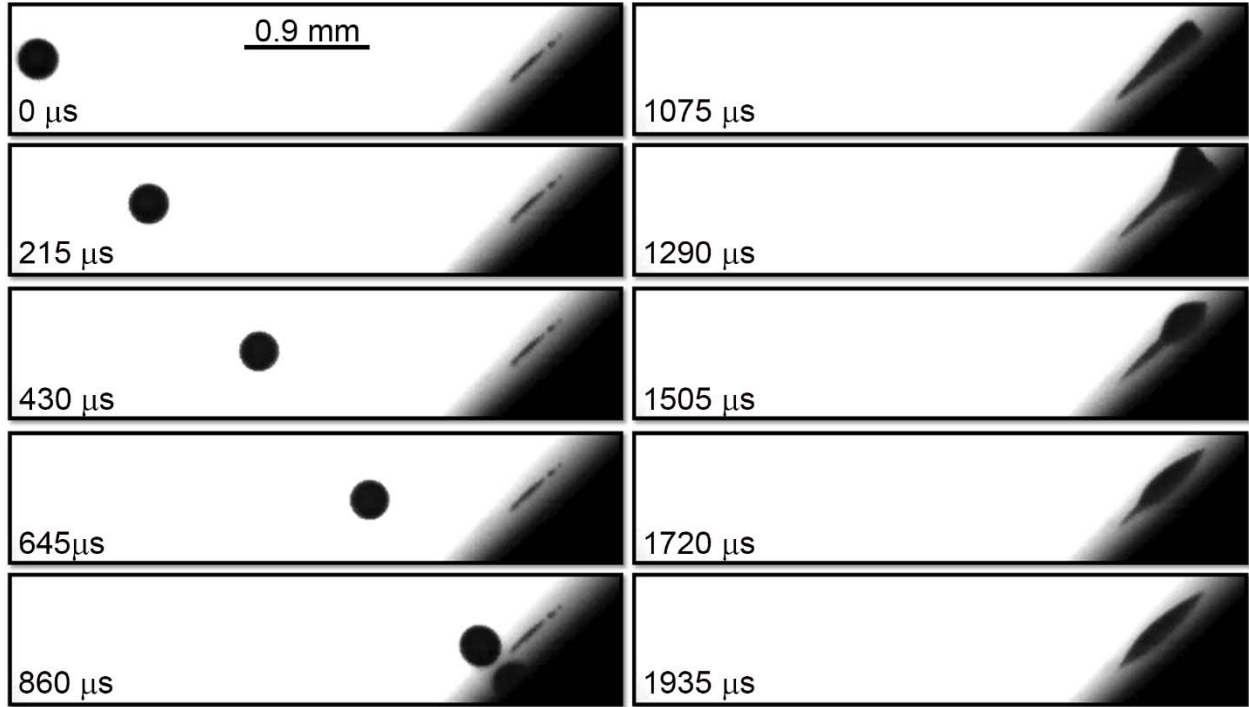


Figure 25: The sequence of image from drop motion to impact on an aluminum surface at 45°. Hematocrit of blood is as: 42±1%

In normal impact, the shape of stain on aluminum surface is usually circular but for some stains shape are neither circular nor elliptical, but lie somewhere in-between. There is no rebound of drop observed onto aluminum surface. It is assumed that the impact process is adiabatic, i.e., there is no heat exchange between the surface and drop.

The basic goal of this measurement is to correlate ratio of stain diameter to drop diameter (D_s/D_d) and ratio of stain volume to drop volume (V_s/V_d) on the base of various size single drop impact on aluminum substrate with various velocity.

Ratio of stain diameter to drop diameter ($\beta=D_s/D_d$):

The measured data of single droplet impact on normal and oblique aluminum substrates was used to correlate the dimensionless maximum spreading diameter ($\beta=D_s/D_d$) of drop with the dimensionless groups characterizing the blood properties and drop velocity.

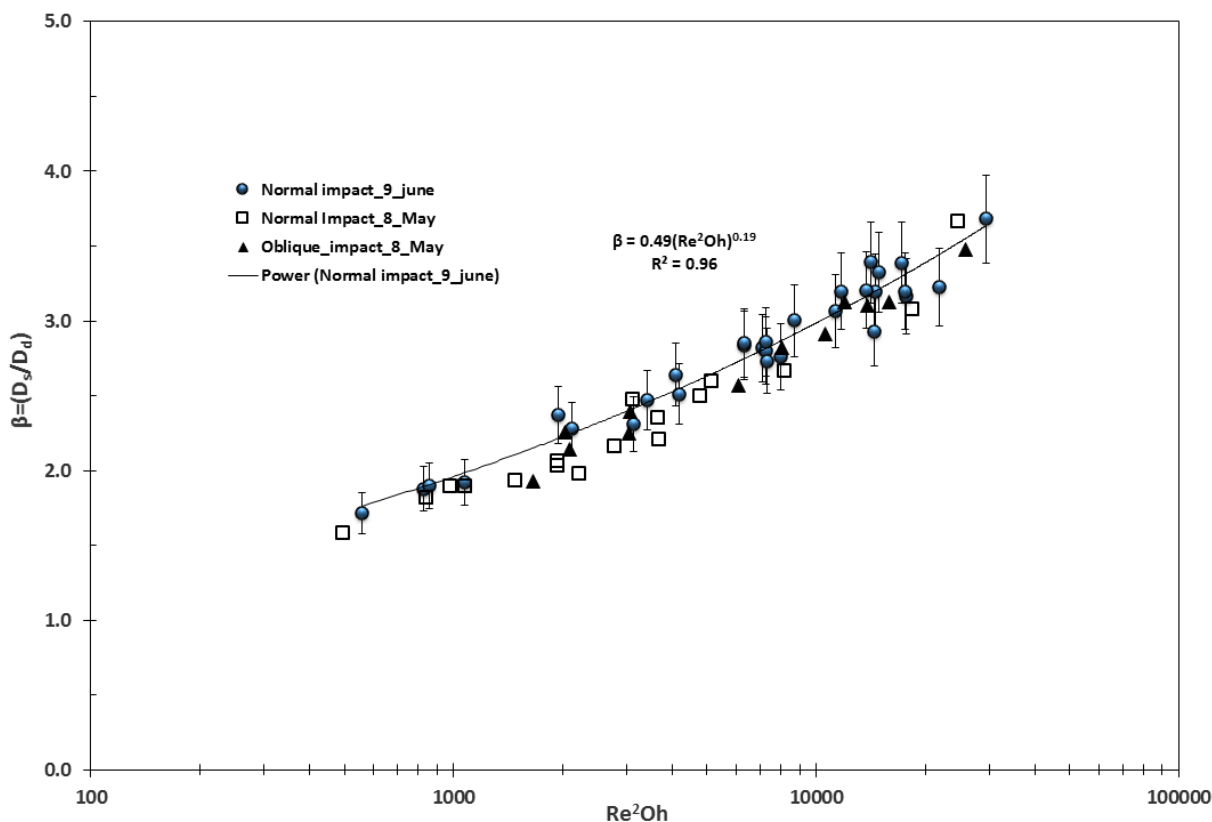


Figure 26: Experimental results for drop impact onto normal and oblique dimensionless maximum spreading diameter correlated against the dimensionless number Re^2Oh . Hematocrit of blood is as: $42 \pm 1\%$

The above figure shows the experimental results of drop impact with the characterizing group Re^2Oh . A regression of maximum spreading diameter with Re^2Oh gives:

$$\beta = \left(\frac{D_s}{D_d} \right) = 0.49 (Re^2 Oh)^{0.19} \quad (10)$$

This expression has a correlation coefficient of 0.96 with the experimental data. All the experiments were carried out at room temperature $24 \pm 2^\circ C$ and relative humidity $40 \pm 3\%$. The maximum error of Re^2Oh is 8%, and the maximum error in β is 5%.

The ratio of stain diameter to drop diameter ($\beta_1 = V_s/V_d$):

The second part of this study concerns the determination of the stain volume to drop volume. The ratio represents a conversion factor to calculate the original volume of drop from the volume of dried stains, see figure below. Some significant deviation ($>10\%$) in β_1 was observed for stains with thickness $<4 \mu m$.

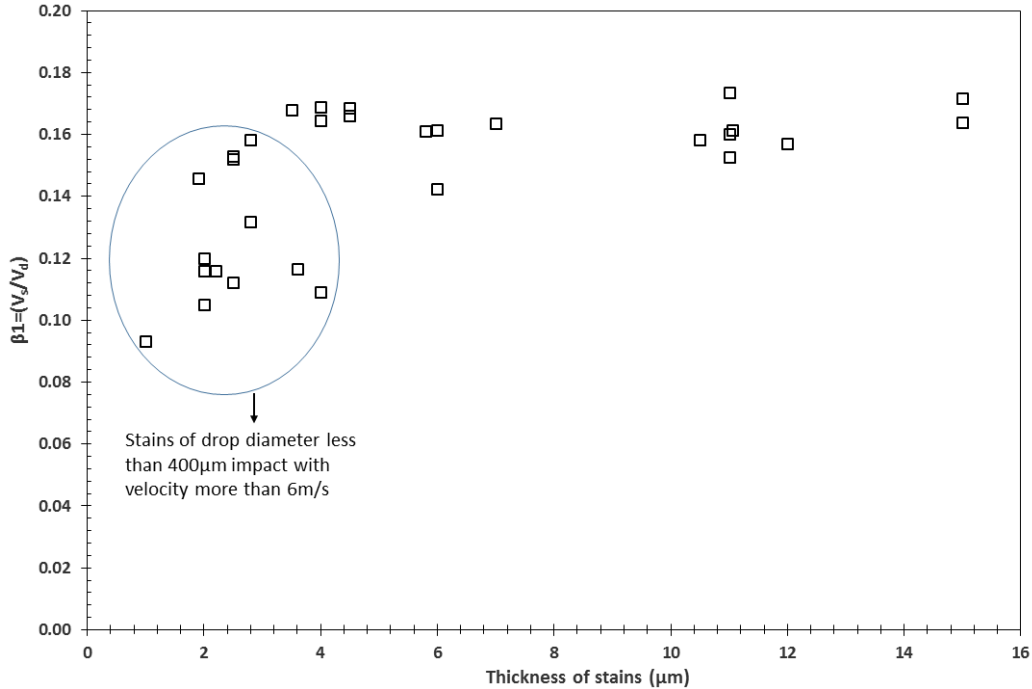


Figure 27: Variation of stain volume to drop volume ratio with respect to stain thickness. Hematocrit of blood is as: $42 \pm 1\%$.

On the bases of impact data, the final correlation of β_1 for stains thicker than $4 \mu\text{m}$ is:
 $\beta_1 \cong 0.16 \pm 5\%$

3.6. Numerical simulation of blood drop impacts

Description of CFD Code Development and InterDyMBlood Release

Within the framework of this grant modifications were made to the standard InterDyMFoam solver to incorporate a physically realistic dynamic wetting model suitable for applications involving blood.

The conventional approach to simulating dynamic wetting conditions is through the use of a “slip model” where the no-slip condition typical to solid boundaries is relaxed in the vicinity of the contact line to allow for slip between the liquid and solid surface [46]. Under axisymmetric conditions, the contact line velocity, u_{CL} , may be explicitly defined from estimates of the local contact angle and an appropriate wetting model, as in Blake and De Coninck [47].

$$u_{CL} = \frac{2K_w \lambda}{\mu} \sinh \left[\frac{\gamma_{LV} \lambda^2}{2k_B T} (\cos \theta_0 - \cos \theta) \right] \quad (11)$$

In the above expression, λ is the adsorption site spacing (O (angstrom)), μ is the dynamic viscosity ($\text{kg m}^{-1}\text{s}^{-1}$), γ_{LV} is the liquid-vapor surface energy (N/m), k_B is the Boltzmann’s constant

($1.3806503 \times 10^{-23} \text{ m}^2\text{kg s}^{-2}\text{K}^{-1}$), T is the absolute temperature (K), θ and θ_0 are the dynamic and static contact angles, and K_w is a parameter used to control the wetting speed, determined through comparison of experimental and numerical results. A value of $\lambda = 2 \times 10^{-10} \text{ m}$ is typically applied for the adsorption site spacing [48], while μ , γ_{LV} and T are physical properties of the fluids and test methodology employed. The static contact angle can be determined through experimental measurement for a broad variety of surfaces, while the value of K_w and corresponding θ vs. u_{CL} must be determined through comparative analysis of simulated and experimental wetting behaviour.

While suitable for two-dimensional or axisymmetric simulations where significant mesh refinement near the target surface can allow for reasonable estimates of θ , the use of the above equation within a 3-dimensional framework poses a few additional challenges. Curvature and contact angle estimates are increasingly sensitive to mesh orientation and structure relative to the advancing surface, requiring prohibitive mesh refinement levels when simulating irregular stains such as those encountered in oblique impact cases. The u_{CL} predicted is also subject to an upper and lower bounds (corresponding to $\theta = 0^\circ$ and $\theta = 180^\circ$), and must be oriented to the contact line's normal direction.

The existing OpenFOAM®'s interDyMFoam solver was extended, where a no-slip velocity boundary was applied on the entire wetted surface and θ is explicitly defined to control the local surface-normal gradient of the volume fraction. This approach offers the advantage of only needing information from the first cells adjacent to the solid surface to define the contact angle (i.e. curvature and near-wall contact line velocity, assumed to be comparable to u_{CL}). Implemented within this framework, the dynamic contact angle was described by the following rearranged form of the above equation:

$$\theta = \cos^{-1} \left[\min \left\{ \max \left\{ \left(\cos \theta_0 - \frac{2k_B T}{\gamma_{LV} \lambda^2} \operatorname{arcsinh} \left[\frac{u_{CL} \mu}{2K_w \lambda} \right] \right), -1 \right\}, 1 \right\} \right] \quad (12)$$

The value of θ defines the vector normal to the interface at the wall, \hat{n} , used to determine interfacial curvature and surface force contributions to the momentum equation:

$$\hat{n} = \hat{n}_w \cos \theta + \hat{n}_t \sin \theta \quad (13)$$

Where \hat{n}_w is the unit normal vector to the surface, oriented towards the surface, and \hat{n}_t is the unit normal vector to the contact line, tangential to the surface and oriented towards the blood droplet. The min and max operations in Eqn. (12) limit the bounds of the contact angle predicted by the inverse cos function to be between 0 and 180° . A potential failure of this methodology may occur when hysteresis is present between the advancing and receding dynamic contact angle. Under these conditions, near-wall curvature can vary significantly between adjacent cells

if there is a sudden flow reversal (i.e. near stagnant conditions), introducing significant localized surface forces and spurious currents. This limitation is relevant to the current simulations of blood impact on rough or absorbent surfaces, where a zero-degree receding contact angle is assumed to approximate the nearly perfect wetting observed for blood due to an increase in viscosity as shear rates decrease. This limitation was addressed in this work by applying Eq. (12) only to the interfacial region, defined by a volume fraction between 0.1 and 0.9, with a 90° contact angle applied elsewhere.

The remaining transport equations and solution algorithm employed within OpenFOAM's interDyMFoam solver have been described in detail elsewhere [49, 50], and will only be described briefly here. The interDyMFoam solver is a VOF sharp interface technique employing the Multidimensional Universal Limited Explicit Solver (MULES) algorithm for interface convection and compression. Movement of the interface between fluids is governed by the evolution of the volume fraction, α .

$$\frac{d\alpha}{dt} + \nabla \cdot (U\alpha) + \nabla \cdot [U_r \alpha (1 - \alpha)] = 0 \quad (14)$$

Where U is the local velocity field and U_r is a relative velocity vector adjusted within the MULES algorithm to limit diffusion of the interface without the use of special convection schemes [49]. Fluid density and viscosity are determined from a volume phase averaging of the distinct phase properties, where a non-Newtonian viscosity model is adopted for blood:

$$\rho = \rho_{blood} \alpha + \rho_{air} (1 - \alpha) \quad (15)$$

$$\mu = \mu_{blood} \alpha + \mu_{air} (1 - \alpha) \quad (16)$$

Momentum transport and continuity were solved assuming incompressible flow and, as discussed later, Newtonian fluid behaviour.

$$\nabla \cdot (\rho U) = 0 \quad (17)$$

$$\frac{\partial \rho U}{\partial t} + \nabla \cdot (\rho U U) = -\nabla p + \nabla \cdot (\mu (\nabla U + \nabla U^T)) + \rho \bar{g} + F_S \quad (18)$$

Surface force contributions to the momentum equation, F_S , were accounted for through the Continuum-Surface-Force Model where the surface normal, \hat{n} , at the wetted surface was determined from Eqn. (3).

$$F_S = -\gamma_{LV} (\nabla \cdot \hat{n}) \nabla \alpha \quad (19)$$

For impact normal to the target substrate, the computational domain was discretized as a hex meshed quarter cylinder with axisymmetric internal boundaries. Simulations were carried out using a Courant number of 0.1 and five levels of dynamic local mesh refinement within the vicinity of the interface (Fig. A). Dynamic wetting was accounted for through a new boundary condition incorporating Eq. (12) to determine the contact angle, θ , at the lower boundary. For oblique impact conditions with a non-zero initial X or Y velocity, a rectangular computational domain was extended for 5 to 10 droplet diameters in the direction of initial droplet motion, with an axisymmetric boundary face bisecting the droplet. The mesh has also be sent up for custom parallelization of the cells within each grid when it is desired to split the simulation onto multiple processor cores. The resulting splitting strategy ensures optimal loads on each processor during dynamic mesh refinement, eliminating the potential for one or two processors to carry the load of the highly refined regions during early stages of the simulation.

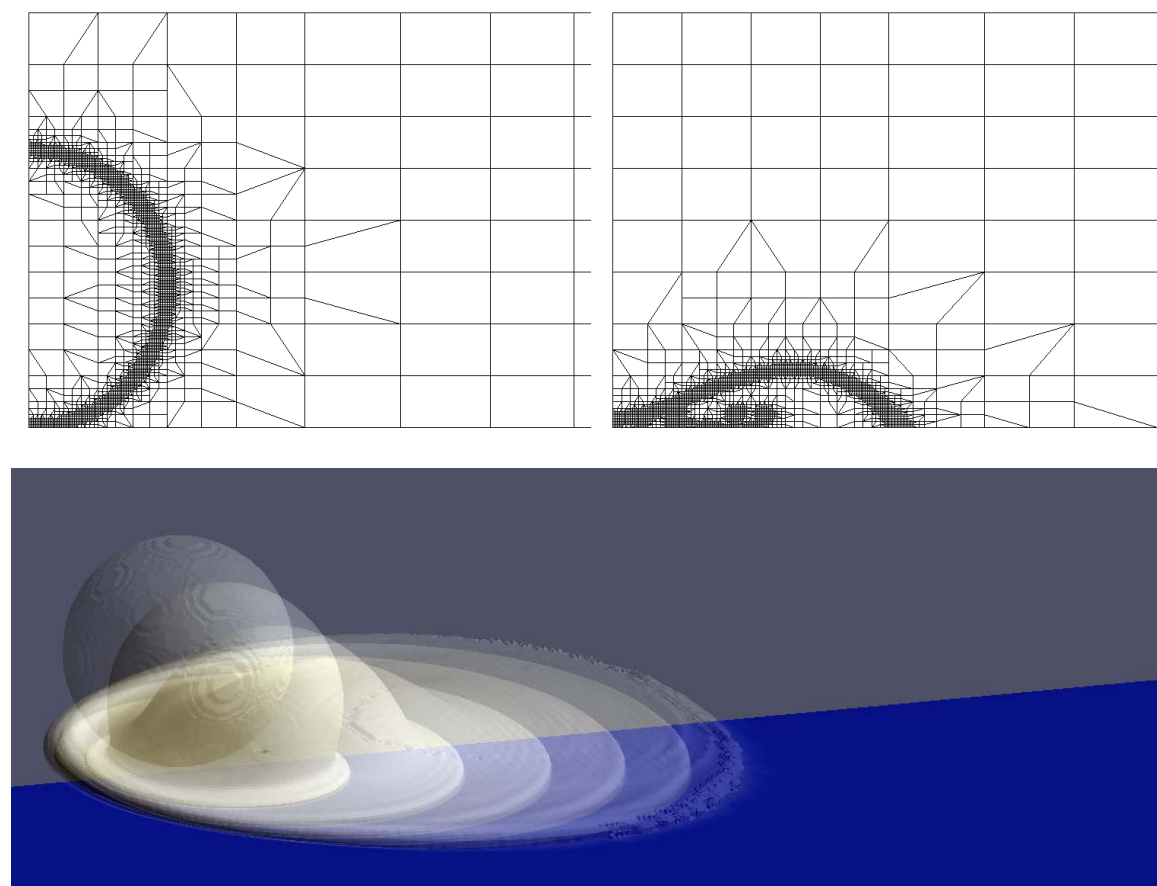


Figure A: View of mesh and interface contour during simulation of blood droplet impact. Note that the mesh dynamically refines during run-time based on the interface position, and the images shown represent the 90° which has been mirrored in both the X and Y axis to provide a 3D image.

Given the relative geometric scale of contact line dynamics to that of the droplet, the level of local mesh refinement and maximum Courant number was varied to determine mesh and time-step independence for an initial coarse single cell volume of approximately 0.216 mm^3 .

Simulations were carried out for a $d_0 = 3.2$ mm water droplet impacting a flat surface at 0.4 m/s for $K_W = 2 \times 10^6$ and 3, 4 and 5 levels of local mesh refinement. At 5 levels of refinement, the characteristic length of a computational cell is reduced to $18.75 \mu\text{m}$, corresponding to a $(2^5)^3$ -fold reduction in cell volume from the coarse mesh (Fig. A). The variation in predicted wetted radius for 4 and 5 levels of mesh refinement was considered acceptable, with a 5 level limit applied in all subsequent simulations. A Courant number of 0.1 was also selected to control temporal discretization errors arising from the explicit scheme inherent to the interDyMFoam solver.

Distributable Software Package

The modified OpenFOAM solver has been prepared for distribution as part of a software package containing the solver, sample cases for both vertical and oblique impact conditions, and a description of required user input variables and execution procedures. A significant requirement for use of this software is the provision of useful physical property data for the blood types used under impact conditions (i.e. a dynamic viscosity model, appropriate physical properties, dynamic wetting parameters, etc.). Prior to release of this code package, we are building a database of suitable parameters for different substrates and blood types through the ongoing experimental work at Iowa State University.

The open-source 3D numerical code presented in section 2.8 has been used to simulate the impact and spreading of blood drops.

Preliminary simulations were carried out for a 45° impact angle, 1.41 m/s impact velocity, density and viscosity comparable to water at ambient conditions, and a static contact angle of 90° . Two surface tensions were employed: 0.07 J/m^2 (Figure 28 left) and 0.007 J/m^2 (Figure 28 right). Laminar conditions were assumed for these initial tests ($\text{Re} \sim 1400$ based on droplet diameter).

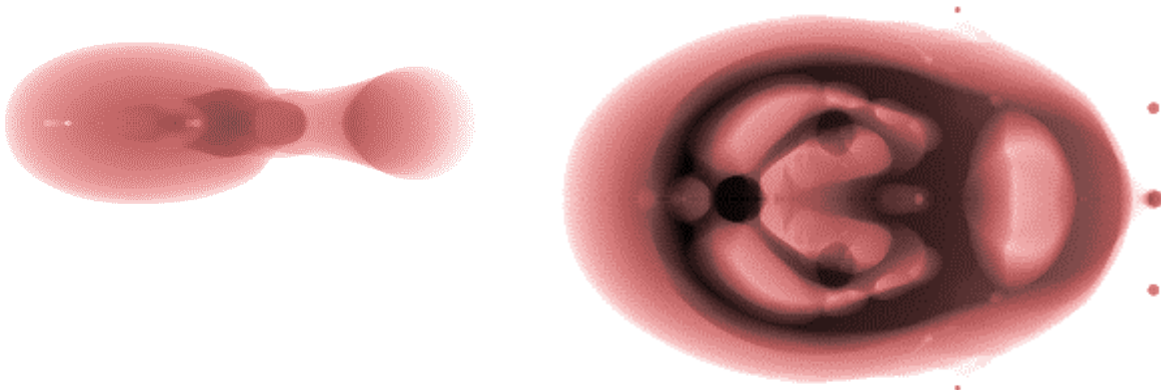


Figure 28. Numerical simulations of time-averaged surface contact areas of an impacting droplet with surface tension of 0.07 J/m^2 (on the left), and 0.007 J/m^2 (right). Darker regions represent extended durations for which the droplet is in direct contact. Note that the droplet impacted from left to right.

Efforts have continued to extend the open-source multi-phase computational fluid dynamics solver to account for blood's complex rheological properties, heat transfer and drying.

The increased viscosity of blood under low shear conditions was found to have a substantial effect on the behavior of a droplet during impact, especially after the droplet initially spreads and starts to relax into its final shape.

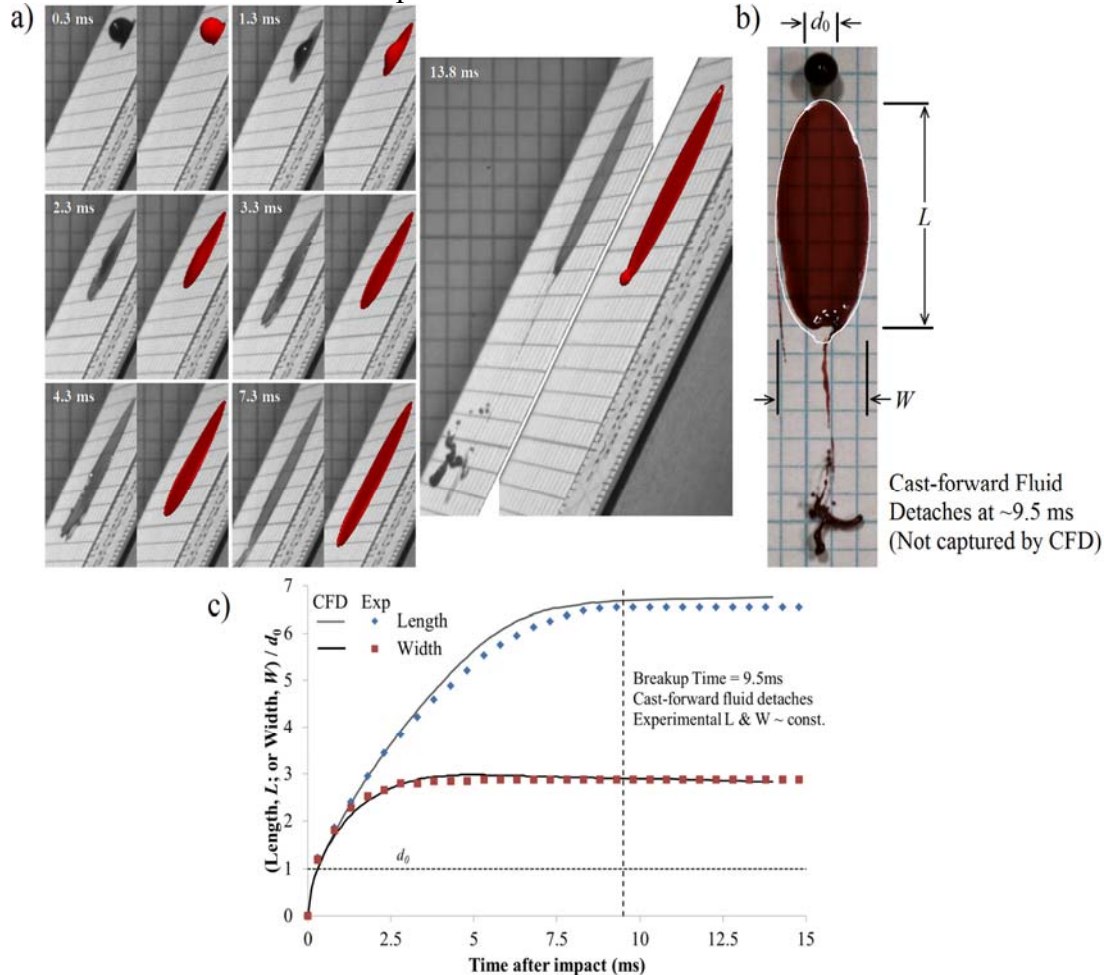


Figure 29. Experiments and computer-based simulations of the oblique impact of a 4 mm human blood droplet (hematocrit unknown) striking a surface at 28° and 4.3 m/s: Comparative droplet shapes (a) of experimental (left and grey) and simulated (right and red) for the indicated times after impact; overlay of simulated (white outline) and experimental drop/stain shape prior-to and 13.8 ms after impact (b); and variation with respect to time of L and W (c). Final experimental W/L elliptical ratio of 0.44 corresponds to $\alpha=26.1^\circ$ using the sine rule. Experiments adapted from the MFRC Bloodstain Pattern Analysis Video Collection, case 4Ac2[51]; simulations from Donaldson and Attinger.

A database of numerical simulations with the 3D droplet impact code have been performed for the impact of pig's blood drops for the following range of conditions, for a total of over 250 simulations:

- Impact Velocities: 1, 2, 5, 7.5, 10, 15, 20 m/s
- Diameters: 200 & 400 μm
- Static Wetting Angle: 5, 30, 60, 90, 105, 140, 170 (in degree)
- Dynamic Wetting Parameter: 10^4 , 10^6 , 10^8

The spread factor (i.e. the ratio between the stain size and the drop size) predicted by the simulations is in very good agreement with the spread factors measured in the experimental study above. The database will be released together with a peer-reviewed manuscript submitted to a technical journal.

Parametric Analysis:

To validate the underlying physical models and numerical framework, simulations were performed for pig blood impacting an aluminum substrate for comparison against experiments performed at Iowa State for high-velocity, low-diameter droplet impact. Droplets ranged from 200 to 400 microns in diameter, with velocities varying from 1 to 20 m/s. The results are illustrated in Figure 30, with the CFD code generally predicting comparable values to the experimental system recognizing that video analysis of droplets of this size makes it challenging to obtain spread factors to within a significant degree of accuracy. The generally accepted correlation of Scheller and Blousfield, $\beta = d_s/d_0 = 0.61(\text{Re}^2\text{Oh})^{0.166}$, consistently overpredicted the spreading of blood droplets and would thus result in an under prediction of Re^2Oh if used to correlate a final stain size to impact conditions, where:

$$\text{Re}^2 \text{Oh} = \frac{\rho^{1.5} d^{1.5} v^2}{\mu \sqrt{\sigma}} \quad (20)$$

With the CFD results appearing promising, simulations were then carried out for contact angles ranging from 10 to 175 degrees and K_w values of 10^4 , 10^6 and 10^8 . The purpose of the parametric analysis was to develop a CFD-based physical model of the spread factor as a function of Re^2Oh , static contact angle and dynamic wetting behavior. From this analysis it was observed that the slope and intercept of a plot of $\ln(\beta)$ vs. $\ln(\text{Re}^2\text{Oh})$ showed a linear dependence on static contact angle with a secondary dependence on K_w (Figure 30). The resulting correlation derived from the CFD results can be expressed as follows:

$$\begin{aligned} \ln \beta &= a_1 + a_2 \ln(\text{Re}^2 \text{Oh}) \\ a_1 &= (-0.8092 + 3.083 \times 10^{-9} K_w) + (5.955 \times 10^{-5} + 4.299 \times 10^{-11} K_w)(180 - \theta_0) \\ a_2 &= (0.1913 + 1.512 \times 10^{-10} K_w) + (8.453 \times 10^{-6} - 4.433 \times 10^{-12} K_w)(180 - \theta_0) \end{aligned} \quad (21)$$

Given the static contact angle of a target surface and a single impact test performed in the field with a device designed to create impact conditions of a known Re^2Oh , the measured β can be used to determine a_1 and a_2 , and subsequently K_w . From this single measurement, a correlation can be established that is fine-tuned the wetting properties of a given surface.

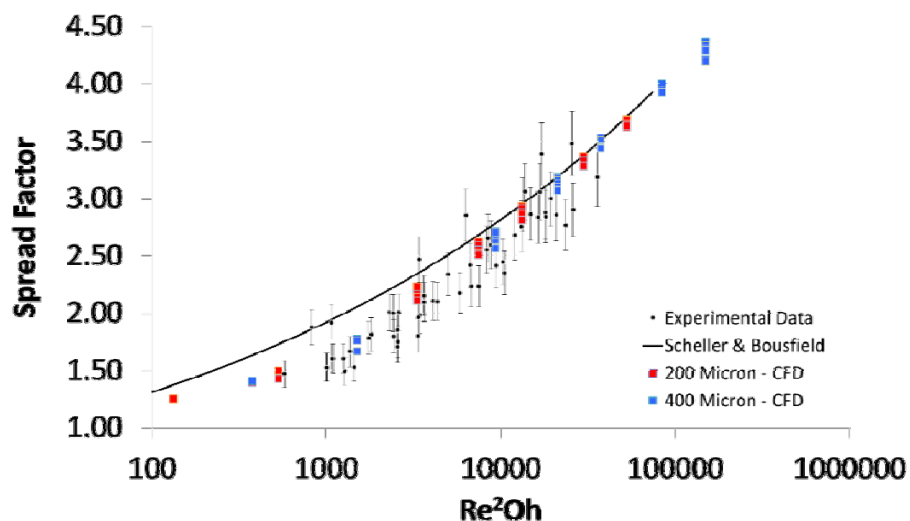


Figure 30: Experimental and simulated spread factors for 200 and 400 micron blood droplets impacting an aluminum surface at velocities ranging from 1 to 20 m/s. A surface tension of 0.059 kg/s² and a viscosity of 3 cP was used in determining Re^2Oh .

Practical Application of the Proposed Model:

To test the practical functionality of the proposed CFD-derived model, additional experiments were performed with larger droplets (2.4 mm) of pig blood striking aluminum ($\theta_0 = 76^\circ$) and cardstock ($\theta_0 = 110^\circ$) surfaces. The pig blood had a slightly higher viscosity at elevated shear (4 cP instead of the 3 cP measured for the blood used for the micrometer droplet trials), and the impact velocities ranged from 0.76 to 4.69 m/s. The experiments were carried out with 5 replicates for each impact velocity. The spread factors obtained at a Re^2Oh of ~ 4000 (5 cm drop height) were then used to determine the K_W values for each substrate which, if incorporated into the proposed model, should describe the spread factor at other impact conditions.

Discussion:

The CFD program developed as part of this collaboration was validated for micron-scale droplet impact conditions when turbulent energy dissipation can be considered negligible relative to surface forces and viscous energy dissipation during impact. A parametric analysis of the spread factors obtained for a variety of contact angles and dynamic wetting conditions yielded the correlation provided in Equation 20, for which the spread factor can be determined for a given Re^2Oh provided the static contact angle and dynamic wetting parameter, K_W , are known. For surfaces with reasonably known static contact angles, a single point measurement of the spread factor on that surface for a controlled Re^2Oh provided sufficient information to determine K_W and reasonably predict the spreading factor at other impact conditions. The CFD simulations provided a lower limit for spreading when a surface was completely non-wetting and the impacting fluid had shear-thinning behavior equivalent to pig blood. With a number of experimental measurements exhibiting spreading lower than this limit when Re^2Oh was

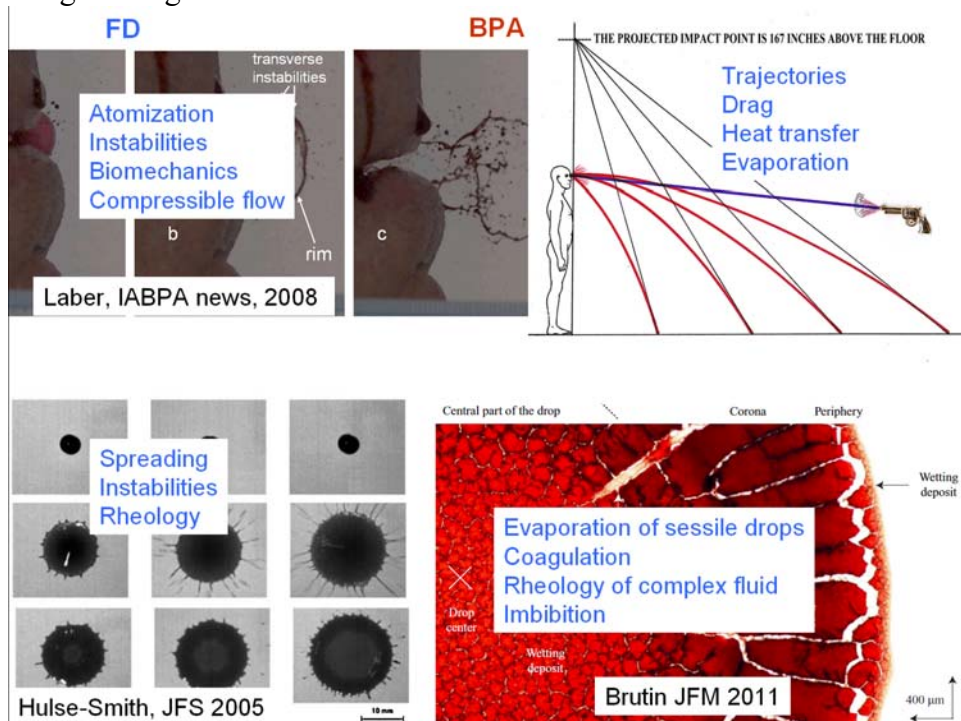
determined from the pendant-drop based surface tension and high shear viscosity, dynamic surface tension and viscoelasticity was explored as potential additional factors responsible.

3.7. Review of the relations between fluid dynamics and bloodstain pattern analysis

A comparative review has been written highlights the relationships between the disciplines of bloodstain pattern analysis (BPA) in forensics and that of fluid dynamics (FD) in the physical sciences. The 22,000-word review paper on the fluid dynamics aspects of bloodstain pattern analysis has been published in a leading forensic journal, Forensic Science International [52]. In both the BPA and FD communities, scientists study the motion and phase change of a liquid in contact with air, or with other liquids or solids. Five aspects of BPA related to FD are discussed: the physical forces driving the motion of blood as a fluid; the generation of the drops; their flight in the air; their impact on solid or liquid surfaces; and the production of stains. For each of the five topics listed above, the review summarizes and review relevant literature from the BPA community, and then from the FD community. In addition, we provide a synthesis of the connections between both disciplines, describing how well the problems are understood and what opportunities exist for new research and the development of novel tools and methods. The findings of our review paper are summarized in a large table including more than 100 citations, which highlights the relations between BPA terminology (rows of the table) and FD concepts (columns).

The review has already been cited 10 times, as of February 10, 2015.

Discussion: The review is part of an effort to create interactions between the fluid dynamics/engineering and BPA communities.



4. Conclusions

1. Discussion of findings.

A method to reconstruct the curved trajectories of blood drops from 3D inspection of blood spatters has been developed. The method works in a laboratory setting, and on very flat substrates (with roughness below 1 micrometer because –stains have typical heights ranging from 5 to 200 micrometer). The 3D microscope used for stain inspection has been modified to possibly be portable to a crime scene. The method has never been tested in a crime scene. The method should be tested the method in a laboratory setting before we release the method. Blood has physical properties (viscosity and surface tension) that have been measured for pig's blood. These properties are extremely complex, with e.g. transient values different than equilibrium values.

2. Implications for policy and practice.

A better method to determine the region of origin of blood spatters has been developed, which is based on sound fluid mechanics principles. This method is about four times more accurate than the current methods based on straight trajectories (method of strings, tangent method, software like Hemospat).

It is unlikely that the method will be used widely in a crime scene in a near future. 3D microscope retail for \$50K, and any surface rougher than 1 micrometer will likely create too much noise in the measurement of stain volumes.

Possibly, the method could be demonstrated on a specific crime scene. For that purpose the following measurements should be taken before the method can be tested:

1. **Measure hematocrit**
2. **Measure ambient conditions (temperature and relative humidity)**
3. **Preserve samples in 3D**

3. Implications for further research.

1. There is a need for more research on the physical properties of blood, and their variation among individuals
2. Blood is a complex fluid that requires thorough characterization and careful manipulation if reproducible results are sought. See for instance recommendations for drop impact experiments in section 2.2.
3. There is a need for measurement methods to determine the volume of a bloodstain that work on a variety of targets, including porous or absorbent targets.
4. The complexity of the physical properties of blood makes it unlikely that satisfactory synthetic substitutes of blood will be found in a near future.

5. References

- [1] "Strengthening Forensic Science in the United States: A Path Forward," Committee on Identifying the Needs of the Forensic Sciences Community, National Research Council 2009.
- [2] V. Balthazard, R. Piedelievre, H. Desoille, and L. Derobert, "Etude des gouttes de sang projete," in *XXIIIe congres de medicine legale de langue francaise*, Paris, 1939.
- [3] P. L. Kirk, *Affidavit Regarding State of Ohio V. Samuel Sheppard*: Court of Common Pleas, Criminal Branch, No. 64571, 26 April 1955.
- [4] N. Behrooz, L. Hulse-Smith, and S. Chandra, "An Evaluation of the Underlying Mechanisms of Bloodstain Pattern Analysis Error," *Journal of Forensic Sciences*, vol. 56, pp. 1136-1142, Sep 2011.
- [5] M. Raymond, E. Smith, and J. Liesegang, "The physical properties of blood – forensic considerations," *Science & Justice*, vol. 36, pp. 153-160, 1996.
- [6] C. D. Adam, "Fundamental studies of bloodstain formation and characteristics," *Forensic Sci Int*, Jan 5 2012.
- [7] C. Knock and M. Davison, "Predicting the position of the source of blood stains for angled impacts," *J Forensic Sci*, vol. 52, pp. 1044-9, Sep 2007.
- [8] M. J. Sweet, "Velocity Measurements of Projected Bloodstains from a Medium Velocity Impact Source," *Journal of Canadian Society of Forensic Science*, vol. 26, pp. 103-110, 1993.
- [9] M. E. Reynolds, M. A. Raymond, and I. Dadour, "The use of small bloodstains in blood source area of origin determinations," *Journal of the Canadian Society of Forensic Science*, vol. 42, pp. 133-146, 2009.
- [10] P. A. Pizzola, S. Roth, and P. R. De Forest, "Blood droplet dynamics. I," *Journal of Forensic Sciences*, vol. 31, pp. 36-49, 1986.
- [11] P. A. Pizzola, S. Roth, and P. R. De Forest, "Blood droplet dynamics. II," *Journal of Forensic Sciences*, vol. 31, pp. 50-64, 1986.
- [12] L. Hulse-Smith, N. Z. Mehdizadeh, and S. Chandra, "Deducing drop size and impact velocity from circular bloodstains," *Journal of Forensic Sciences*, vol. 50, pp. 54-63, 2005.
- [13] M. El-Sayed, D. A. C. Brownson, and C. E. Banks, "Crime scene investigation II: The effect of warfarin on bloodstain pattern analysis," *Analytical Methods*, vol. 3, pp. 1521-1524, 2011.
- [14] D. A. C. Brownson and C. E. Banks, "Crime scene investigation: The effect of drug contaminated bloodstains on bloodstain pattern analysis," *Analytical Methods*, vol. 2, pp. 1885-1889, 2010.
- [15] M. A. Raymond and R. L. H. Raymond, "An Interesting Application of Infrared Reflection Photography to Blood Splash Pattern Interpretation," *Forensic Science International*, vol. 31, 1986.
- [16] M. A. Raymond, E. R. Smith, and J. Liesegang, "Oscillating blood droplets - implications for crime scene reconstruction," *Science and Justice - Journal of the Forensic Science Society*, vol. 36, pp. 161-171, 1996.

- [17] D. Attinger, C. Moore, A. Donaldson, A. Jafari, and H. A. Stone, "Fluid dynamics topics in bloodstain pattern analysis: comparative review and research opportunities," *Forensic Sci Int*, vol. 231, pp. 375-96, 2013.
- [18] B. L. Scheller and D. W. Bousfield, "Newtonian drop impact with a solid surface," *Aiche Journal*, vol. 41, pp. 1357-1367, 1995.
- [19] M. B. Illes, "Investigation of a model for stain selection and a robust estimation for area of origin in bloodstain pattern analysis," MS Thesis, Trent University, Ontario, Canada, 2011.
- [20] A. L. Carter, M. Illes, K. Maloney, A. B. Yamashita, B. Allen, B. Brown, L. Davidson, G. Ellis, J. Gallant, A. Gradkowski, J. Hignell, S. Jory, P. L. Laturmus, C. C. Moore, R. Pembroke, A. Richard, R. Spenard, and C. Stewart, "Further Validation of the BackTrack(TM) Computer Program for Bloodstain Pattern Analysis: Precision and Accuracy," *International Association of Bloodstain Pattern Analysts News*, vol. 21, pp. 15-22, 2005.
- [21] K. G. de Bruin, R. D. Stoel, and J. C. M. Limborgh, "Improving the Point of Origin Determination in Bloodstain Pattern Analysis," *Journal of Forensic Sciences*, vol. 56, pp. 1476-1482, 2011.
- [22] U. Buck, B. Kneubuehl, S. Näther, N. Albertini, L. Schmidt, and M. Thali, "3D bloodstain pattern analysis: ballistic reconstruction of the trajectories of blood drops and determination of the centres of origin of the bloodstains," *Forensic Sci Int*, vol. 206, pp. 22-8, Mar 20 2011.
- [23] B. T. Cecchetto, "Nonlinear Blood Pattern Reconstruction," MS thesis, The University of British Columbia, Vancouver, Canada, 2010.
- [24] P. A. Pizzola, J. M. Buszka, N. Marin, N. D. K. Petraco, and P. R. De Forest, "Commentary on "3D bloodstain pattern analysis: Ballistic reconstruction of the trajectories of blood drops and determination of the centres of origin of the bloodstains" by Buck et al. [Forensic Sci. Int. 206 (2011) 22-28]," *Forensic Sci Int*, vol. 220, pp. e39-e40, 2012.
- [25] C. R. Varney and F. Gittes, "Locating the source of projectile fluid droplets," *American Journal of Physics*, vol. 79, pp. 838-842, 2011.
- [26] E. J. Lavernia, E. M. Gutierrez, J. Szekely, and N. J. Grant, "A mathematical model for the liquid dynamic compaction process. Part 1: Heat flow in gas atomization," *Int. J. Rapid Solid.*, vol. 4, pp. 89-124, 1988.
- [27] D. Attinger, C. Moore, C. Frankiewicz, B. Sikarwar, and A. Donaldson, "Can we reconstruct the curved trajectories of blood drops?," *Forensic Science International*, (in preparation, 2015).
- [28] D. Attinger, C. Moore, and C. Frankiewicz, "Can we reconstruct the curved trajectories of blood drops?," in *IABPA (international association of bloodstain pattern analysts) training conference*, San Diego, CA, 2013.
- [29] D. Attinger, C. Moore, A. Donaldson, and H. A. Stone, "Fluid Dynamics Aspects of Bloodstain Pattern Analysis: Comparative review and research opportunities," in *IABPA (international association of bloodstain pattern analysts) training conference*, San Diego, CA, 2013.
- [30] N. Laan, R. H. Bremmer, M. C. Aalders, and K. G. de Bruin, "Volume determination of fresh and dried bloodstains by means of optical coherence tomography," *J Forensic Sci*, vol. 59, pp. 34-41, Jan 2014.

- [31] N. Kim, Z. Li, C. Hurth, F. Zenhausern, S.-F. Chang, and D. Attinger, "Identification of fluid and substrate chemistry based on automatic pattern recognition of stains," *Analytical Methods*, vol. 4, pp. 50-57, 2012.
- [32] C. A. Schneider, W. S. Rasband, and K. W. Eliceiri, "NIH Image to ImageJ: 25 years of image analysis," *Nature Methods*, vol. 9, pp. 671-675, 2012.
- [33] C. Tropea, A. L. Yarin, and J. F. Foss, *Springer Handbook of Experimental Fluid Mechanics*: Springer, Heidelberg, Germany, 2007.
- [34] J. F. Steffe, *Rheological Methods in Food Process Engineering*: Freeman Press, 1996.
- [35] M. D. Misak, "Equations for determining $1/H$ versus S value in computer calculations of interfacial tension by pendant drop method," *J. Colloid Interface Science*, vol. 27, pp. 141-142, 1968.
- [36] A. Ghosh, B. S. Sikarwar, and D. Attinger, "Microfluidic Measurements of Physical Properties of Blood for Forensic Studies," presented at the 2014 International ASME Conference on Nanochannels, Minichannels and Microchannels, Chicago IL, 2014.
- [37] B. S. Sikarwar, A. Ghosh, and D. Attinger, "Simple, Low Cost Microfluidic Measurements of Physical Properties of Blood for Forensic Studies,," presented at the 2014 International ASME Conference on Nanochannels, Minichannels and Microchannels, Chicago IL, 2014.
- [38] C. E. Stauffer, "The Measurement of Surface Tension by the Pendant Drop Technique," *Journal Phys. Chemistry*, vol. 69, p. 6, 1965.
- [39] S. Kim, Y. Ma, P. Agrawal, and D. Attinger, "How important is it to consider target properties and hematocrit in bloodstain pattern analysis?," *Forensic Science International*, 2016 (under revision).
- [40] A. Kolbasov, P. Comiskey, R. P. Sahu, S. Sinha-Ray, A. L. Yarin, B. S. Sikarwar, S. Kim, T. Z. Jubery, and D. Attinger, "Blood Rheology in Shear and Uniaxial Elongation," *Rheological Acta*, submitted 2016.
- [41] R. J. Poole and B. S. Ridley, "Development-length requirements for fully developed Laminar pipe flow of inelastic non-Newtonian liquids," *Journal of Fluids Engineering-Transactions of the Asme*, vol. 129, pp. 1281-1287, Oct 2007.
- [42] C. Hurth, R. Bhardwaj, C. Frankiewicz, A. Dobos, D. Attinger, and F. Zenhausern, "Biomolecular interactions control coffee ring effect during droplet drying," *Colloids and Surfaces B: Biointerfaces*, submitted Dec 2014.
- [43] N. Laan, K. G. de Bruin, D. Bartolo, C. Josserand, and D. Bonn, "Maximum Diameter of Impacting Liquid Droplets," *Physical Review Applied*, vol. 2, 2014.
- [44] L. I. Meho and K. Yang, "Impact of data sources on citation counts and rankings of LIS faculty: Web of science versus scopus and google scholar," *Journal of the American Society for Information Science and Technology*, vol. 58, pp. 2105-2125, Nov 2007.
- [45] R. F. Allen, "The role of surface tension in splashing," *Journal of Colloid and Interface Science*, vol. 51, pp. 350-351, 1975.
- [46] R. Bhardwaj and D. Attinger, "Non-isothermal wetting during impact of millimeter-size water drop on a flat substrate: Numerical investigation and comparison with high-speed visualization experiments," *International Journal of Heat and Fluid Flow*, vol. 29, pp. 1422-1435, 2008.
- [47] T. D. Blake and J. De Coninck, "The influence of solid-liquid interactions on dynamic wetting," *Advances in Colloid and Interface Science*, vol. 96, pp. 21-36, 2/25/ 2002.

- [48] M. Dietzel and D. Poulikakos, "Laser-induced motion in nanoparticle suspension droplets on a surface," *Physics of Fluids*, vol. 17, p. 102106, 2005.
- [49] E. Berberović, N. van Hinsberg, S. Jakirlić, I. Roisman, and C. Tropea, "Drop impact onto a liquid layer of finite thickness: Dynamics of the cavity evolution," *Physical Review E*, vol. 79, 2009.
- [50] OpenCFD. (2013). *OpenFOAM 2.2.0: User Guide*. Available: <http://www.openfoam.org/docs/user/index.php>
- [51] T. L. Laber, B. P. Epstein, and M. C. Taylor. *High speed digital video analysis of bloodstain pattern formation from common bloodletting mechanisms, Bloodstain Pattern Analysis Video Collection, Midwest Forensic Center (Ames, IA)*. Available: www.mfrc.ameslab.gov
- [52] D. Attinger, C. Moore, A. Donaldson, A. Jafari, and H. A. Stone, "Fluid dynamics topics in bloodstain pattern analysis: Comparative review and research opportunities," *Forensic Science International*, vol. DOI <http://dx.doi.org/10.1016/j.forsciint.2013.04.018>, pp. 375-396, 2013.
- [53] D. Attinger, B. S. Sikarwar, C. Frankiewicz, and C. Moore, "On the importance of drop impact studies in forensic applications," presented at the 2014 International ASME Fluids Engineering Conference, August 2014 (invited presentation).
- [54] D. Attinger, "On the importance of drop impact studies in forensic applications (invited lecture)," presented at the 2014 International ASME Fluids Engineering Conference, Chicago IL, 2014.
- [55] D. Attinger, C. Moore, A. Donaldson, A. Jafari, and H. Stone, "Opportunities for Fluid Dynamics Research in the Forensic Discipline of Bloodstain Pattern Analysis," *Bulletin of the American Physical Society*, vol. 58, 2013.
- [56] A. Jafari, Y. Xing, C. Moore, A. Donaldson, H. Stone, and D. Attinger, "On Some Fluid Dynamics and Heat Transfer Aspects of Bloodstain Pattern Analysis in Forensics," in *ASME Heat Transfer Conference*, Minneapolis, Minnesota, 2013.
- [57] A. Donaldson and D. Attinger, "An Open Source, Dynamic Wetting Code for the Impact of Blood Droplets, with Relevance to the Forensic Discipline of Bloodstain Pattern Analysis, ICNMM2013-73166," in *11th ASME International Conference on Nanochannels, Microchannels and Minichannels (ICNMM)*, Sapporo, Japan, 2013.

6. Dissemination of Research Findings

The general dissemination strategy in this grant is to create opportunities for two communities of interest (fluid dynamics and bloodstain pattern analysis) to be aware of the other community and to understand that together they can find and solve innovative problems with relevance to BPA. This strategy is summarized in Figure 32 and described in more details right after.

The following material has been disseminated by submissions and publications in peer reviewed, leading journals of forensic science: the critical review on BPA and fluid dynamics[17]; the influence of target properties on trajectory reconstruction [39]; the measurement of viscosity[40].

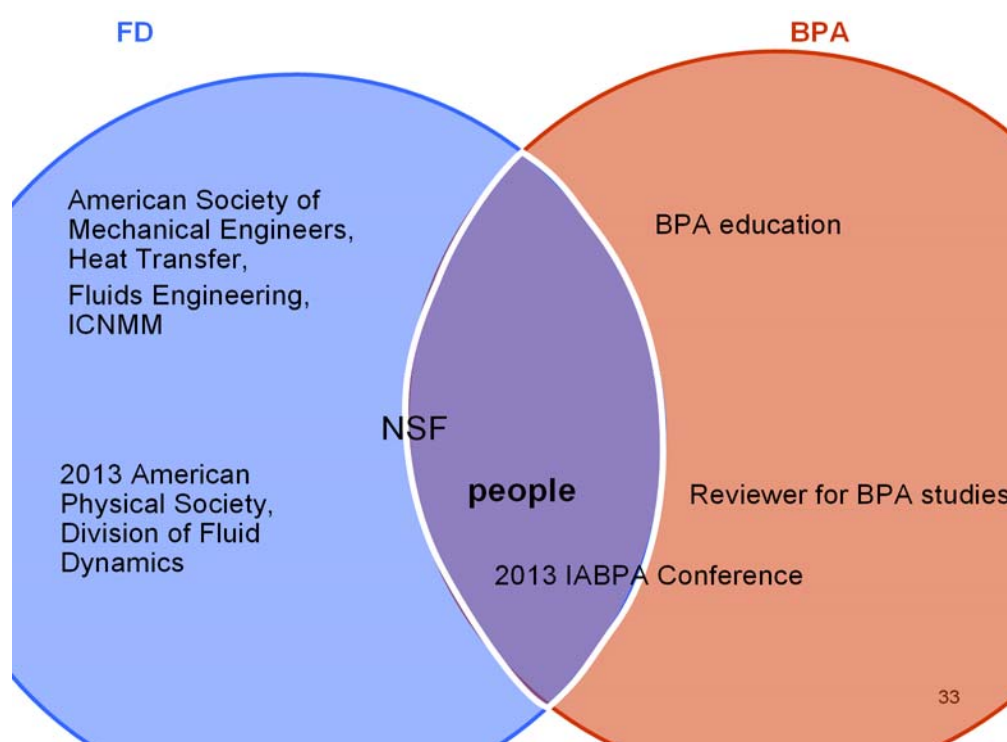


Figure 32: Activities of Attinger regarding the construction of contacts between the BPA and Fluid Dynamics (FD) communities. These dissemination activities include the presentation of BPA challenges and background at engineering and physics conference, the delivery of a 1 hour lecture on fluid dynamics at the major BPA conference (BPA), the design of an education plan for BPA experts who want to learn fluid dynamics (see also Annex), and serving more than 10 times as a reviewer for the leading forensic journal “Forensic Science International”.

Attinger was invited to give two lectures (1hr 30 minutes total) in the major international conference on Bloodstain Pattern Analysis (2013 IABPA). One of the lectures was on the connections between BPA and fluid dynamics. The general atmosphere at the IABPA conference was that fluid dynamics challenges in BPA are currently being identified and will take at least 10 years to be addressed. For instance, the group of Mike Taylor presented a study showing the lack of measurements of blood properties in even the most cited BPA studies (see also section A32 above), and the consequences of this neglect, in terms of experimental uncertainty and difficulty to perform comparisons between BPA studies.

A presentation entitled “*Review on some Fluid Dynamics Aspects of Bloodstain Pattern Analysis*” has been given February 18, 2014, to the AAFS/NIJ grantee conference, “Our Trail Onward: Mentoring the Next Generation of Researchers in Forensic Science”. Questions in the audience were about the release of the computational fluid dynamic drop impact tool, and the portability of the trajectory reconstruction method to a crime scene.

A presentation on our BPA research has also been given to the group of Paul Yager University of Washington Seattle, February 20, 2014. The group specializes in microfluidics methods for medical applications.

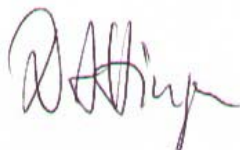
Several conference presentations and one poster have been prepared for the following two conferences: ASME ICNMM conference and ASME FED conference, which are being collocated in Chicago, August 4-8, 2014 [36, 37, 53, 54].

During the summer 2014, I was invited as a visiting professor at Tsinghua University, the leading university of science and technology of China. I took the opportunity to contact several groups doing forensics in Beijing, and was invited to the Beijing Forensic Medicine, June 25, 2014. The visit was hosted by Dr. Jianhua Chen, Professor at the Beijing Forensic Science Institute, and Mr. Li Liu, the Director of the Forensic Medical Center. Presentation was given of the invited lecture "*Bloodstain Pattern Analysis: A roadmap towards more practical and accurate methods*". I was very impressed to have every one of my sentences translated orally in Mandarin Chinese. I was also given a tour of the Medicine Center Facilities. I found out that forensic scientists in China also have doubts on the current state of the art of Bloodstain Pattern Analysis.

Attinger also presented on the connections between BPA and fluid dynamics to a broad audience of more than 60 persons at the Cafe Scientifique of the Science Center of Iowa, on October 8, 2013.

We gave technical talks [55-57], at three engineering conferences. These conferences were the Division of Fluid Dynamics of the American Physical Society, the world best conference on fluid dynamics; The International Conference on Mini, Micro and Nanochannels, an engineering conference on thermal-fluid topics that Attinger will chair in summer 2014; and the summer heat transfer conference of the American Society of Mechanical Engineers, the largest US conference on thermofluid topics.

Signature of Submitting Official:

A handwritten signature in dark ink, appearing to read "D. Attinger". The signature is fluid and cursive, with the first name "D." and last name "Attinger" clearly distinguishable.

Dr. Daniel Attinger, Ames IA, July 29, 2015 and
updated April 19 2016